



*Annual Review of Earth and Planetary Sciences*

# Pleistocene Periglacial Processes and Landforms, Mid-Atlantic Region, Eastern United States

Dorothy J. Merritts and Michael A. Rahnis

Department of Earth and Environment, Franklin and Marshall College, Lancaster, Pennsylvania; email: dmerritt@fandm.edu

Annu. Rev. Earth Planet. Sci. 2022. 50:541–92

The *Annual Review of Earth and Planetary Sciences* is online at [earth.annualreviews.org](http://earth.annualreviews.org)

<https://doi.org/10.1146/annurev-earth-032320-102849>

Copyright © 2022 by Annual Reviews.  
All rights reserved

## Keywords

periglacial, permafrost, solifluction, thermal contraction crack polygons, colluvium, frost cracking

## Abstract

Just as glaciers worldwide left a record of past advances and retreats that shifted latitudinally in response to oscillating Quaternary climate changes, so too have cold-climate conditions and permafrost left topographic and sedimentary signatures in former periglacial environments. This review documents widespread occurrence of past permafrost and intense frost action that led to rock fracturing, regolith production, and regolith-mantled slopes in the mid-Atlantic region of the United States during late Pleistocene cold-climate conditions. Strong signatures of thermal contraction cracking and brecciation from frost cracking exist where rocks and sediments are most frost susceptible, as with fissile shales. On sandstone hillslopes, frost weathering produced boulder-rich sediment that episodically flowed slowly downslope during permafrost thaw, resulting in solifluction lobes and terraces in which colluvium moved cumulatively at least a kilometer. Radiocarbon dating, optically stimulated luminescence age control, and cosmogenic isotope studies constrain some periglacial features to the Last Glacial Maximum but also indicate longer residence times of regolith.

- Former permafrost and areas of intensive frost cracking extended over much of the mid-Atlantic region of the eastern United States during late Pleistocene cold glacial periods.



- Cold-climate conditions and permafrost left long-lasting topographic and sedimentary records with limited post-depositional erosion in the formerly periglacial mid-Atlantic region.
- Prominent relict periglacial landforms include polygon networks and frost wedges that are the result of thermal contraction cracking and brecciated rock formed by segregated ice and frost cracking.
- Widespread solifluction landforms are a topographic signature of freezing, thawing, and mass movement of mobile regolith produced by frost cracking, and some were active during the Last Glacial Maximum.

## INTRODUCTION

The focus of this review is Pleistocene periglaciation of landscapes in the mid-Atlantic region (MAR) of the unglaciated eastern United States, a slow-eroding setting between the latitudes of approximately 41 and 39°N (**Figure 1a**). This review highlights bedrock landscapes in the Appalachian Mountains and Piedmont, where evidence of patterned ground, frost wedges, and periglacial slope processes is pervasive. Airborne lidar data acquired since about 2004 reveal lobate forms that are ubiquitous on hillslopes with boulder colluvium and likely from widespread Pleistocene solifluction, a form of slow mass movement associated with freeze-thaw processes (Merritts et al. 2013, 2020; Del Vecchio et al. 2018) (**Figures 2** and **3**). Nevertheless, questions remain about whether, where, and when past permafrost existed in this landscape (Péwé 1983, French & Millar 2014, Merritts et al. 2020). Because permafrost exerts fundamental controls on depth, type, and efficiency of weathering and hillslope processes (Goodfellow & Boelhouwers 2013), determining its former presence and extent is of consequence. Modeling of the extent and magnitude of frost weathering during the Last Glacial Maximum (LGM; ~27–19 ka BP) (Clark et al. 2009) shows that intense frost cracking might have extended much farther south throughout North America (Marshall et al. 2021) and affected a significantly greater area than that of the mapped LGM permafrost extent (French & Millar 2014) (**Figure 1b**).

Some periglacial features of the Mid-Atlantic Coastal Plain (MACP) are described here because of their significance for better understanding of the southernmost extent of permafrost during the LGM. However, the Coastal Plain's relatively low altitude and relief, unconsolidated Cenozoic sediments, and maritime location result in notable differences in periglacial history compared to the higher elevation bedrock landscapes farther inland that are emphasized in this review.

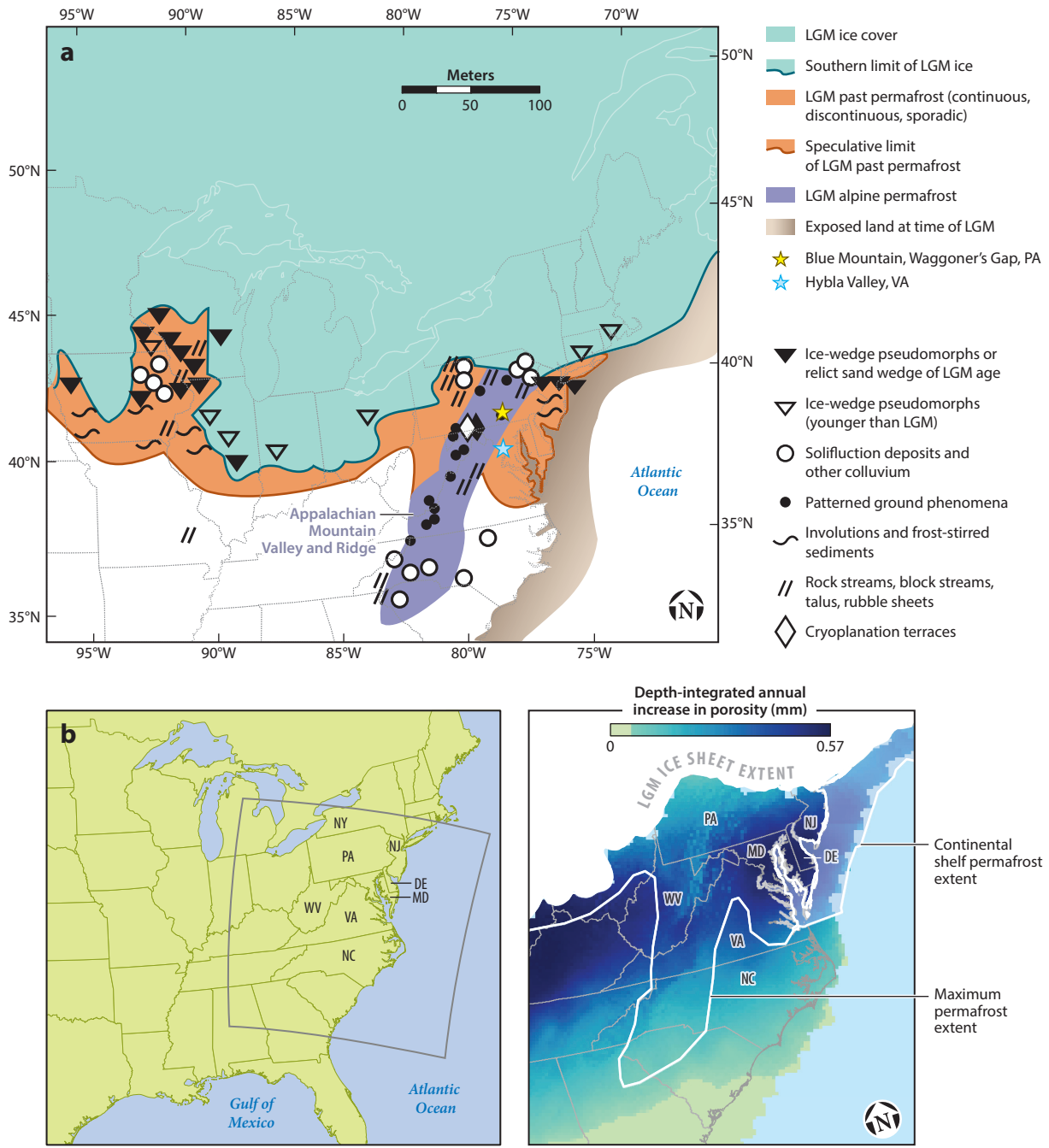
The broad sweep of discovery of periglacial features in the MAR spans from early reports of vast, barren block deposits to current understanding of the region's landscape history in response to oscillating Quaternary cold-climate conditions. Such understanding is relevant to modern studies of landscape response to warming and permafrost thaw (Gooseff et al. 2009, Rowland et al. 2010). Establishing the rates at which frost processes convert bedrock to regolith and transport it downslope is an area of active research in geomorphology (e.g., Hales & Roering 2007, 2009; Anderson et al. 2013, 2015; Egholm et al. 2015; Rempel et al. 2016). Studies in the Oregon Coast Range, for example, document cosmogenic-derived erosion rates at least 2.5 times greater during the LGM periglacial conditions compared to modern interglacial conditions (Marshall et al. 2015, 2017).

### What Is Periglacial?

The word periglacial, technically meaning near glacial, is used in conjunction with geomorphology, landscapes, and processes, among other pairings. Periglacial geomorphology focuses on



landscapes shaped by cold-climate nonglacial conditions and ground freezing, at present or in the past and regardless of proximity to glaciers (Thorn 1992, French 2017b). The first known use of the word periglacial was in 1909, when Polish geographer Walery von Łoziński described mechanical disintegration of sandstones in the mid-latitude Carpathian Mountains south of the



(Caption appears on following page)



**Figure 1** (Figure appears on preceding page)

(a) Extent of past permafrost south of the limit of Last Glacial Maximum (LGM) ice for the eastern United States (*b*), based on compilation of periglacial features. For simplicity, some periglacial features north of the LGM ice margin in Canada are not included. Waggoner's Gap on Blue Mountain is located near the relict sand wedge referred to in the text and **Table 3** (see **Figure 11c**). The piedmont lies to the southeast of the Valley and Ridge along its length. Map adapted from French & Millar (2014), which was derived from Péwé (1983), figure 9.11. (*b*) Predicted extent and magnitude of depth-integrated annual increase in frost weathering (modeled as depth-integrated increase in porosity). Figure adapted from Marshall et al. (2021); LGM permafrost extent from Lindgren et al. (2016); ice sheet extent from Dyke et al. (2003).

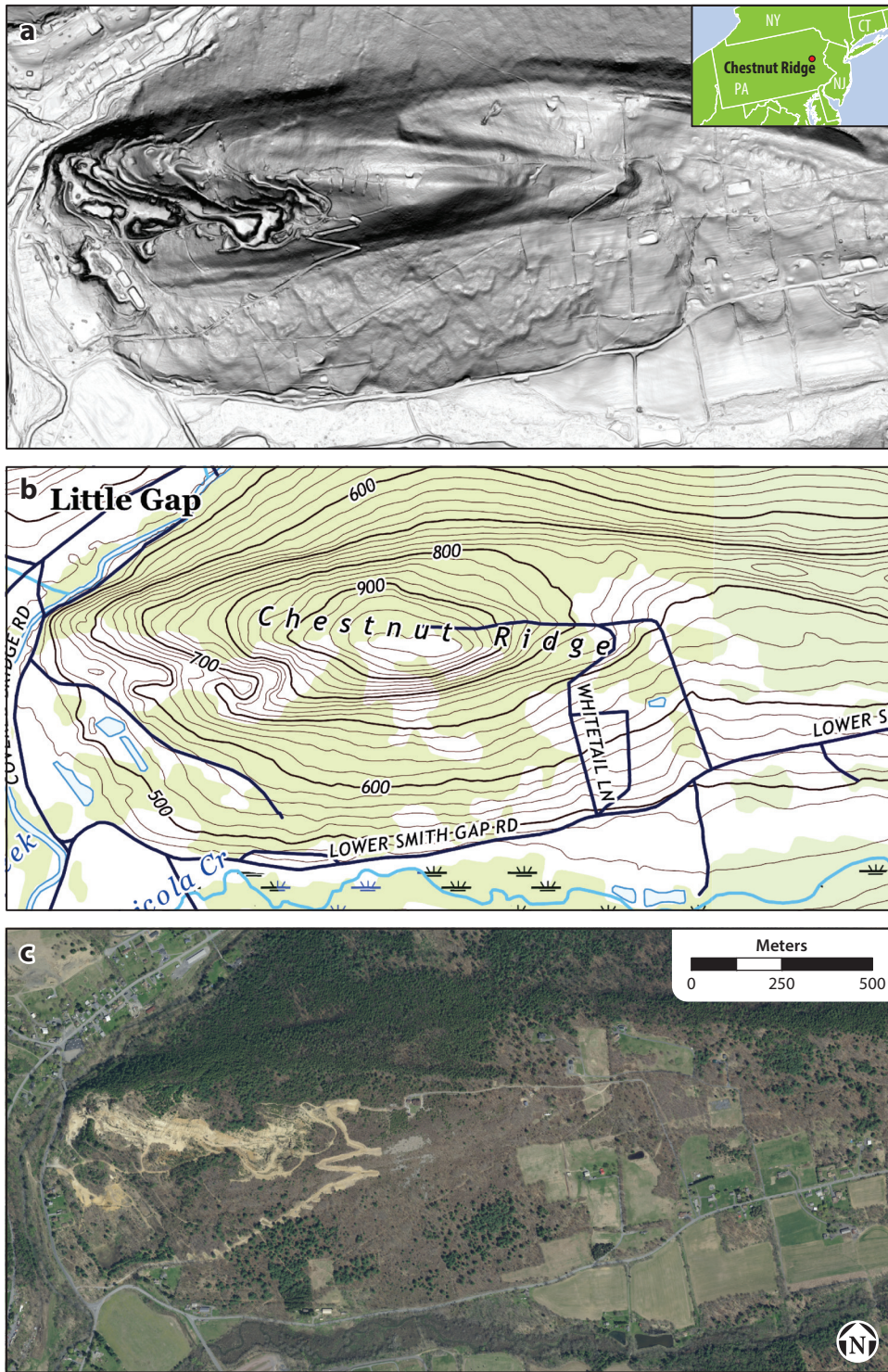
southernmost extent of glaciation from former continental ice sheets in Europe (von Łozinski 1909, French 2000). von Łozinski described blockfields of boulder-sized angular sediment as a periglacial facies produced by frost action during severe cold conditions (von Łozinski 1912, French 2000). Interpreting their origin as the result of intensive frost splitting during formerly cold periods, he referred to the detritus as frost rubble (von Łozinski 1909, French 2000). Soon after, the word periglacial was used in reference to a zone of cold-climate conditions and geomorphic processes peripheral to Pleistocene ice masses.

French (2000) inferred that von Łozinski probably was influenced by Swedish archaeologist and geologist Johan G. Andersson's contemporaneous work in high-latitude cold landscapes. Andersson (1906) had observed active mass wasting in the North Atlantic region (Norwegian Svalbard archipelago, 74°26') and what appeared to be inactive mass movement deposits (i.e., relict) in the South Atlantic Falkland Islands (52°S). For the Falkland Islands, Andersson described low-gradient (typically less than 8 to 10°) stone runs and stone rivers that consisted of quartzite blockfields up to several kilometers in width along hillslopes and valley bottoms. Earlier visits to the Falkland Islands by Charles Darwin and Sir Wyville Thomson led to vivid descriptions of the features as "pale-gray glistening masses...which look...much like glaciers descending apparently from the adjacent ridges" (Thomson 1878, p. 245). Others noted the resemblance of these blocky features to rubble drift and head deposits in southern England, now recognized as relict periglacial features (Geikie 1894, Ballantyne & Harris 1994, French 2000, Ballantyne 2018). By the mid-twentieth century, geologists in the MAR were reporting on similar rubble deposits and comparing them to modern cold-climate features (Peltier 1950, Denny 1951, Potter & Moss 1968, Moss 1976).

Andersson's keen observations and descriptions of cold-region landforms and processes continue to influence modern thinking in periglacial geomorphology. He is credited with introducing the term solifluction (*solum* from soil and *fluere* from to flow) to describe phenomena he saw on Bear Island (74°N) in the Norwegian Svalbard archipelago (Andersson 1906). There, he observed the slow movement of "semifluid...masses of waste saturated with water" downslope due to recurrent ground freezing and thawing, perhaps enhanced by underlying frozen ground (Andersson 1906) (see **Figure 3**). Andersson attributed the relict stone runs of the Falkland Islands to the same process of solifluction, albeit in the past, noting that based on his earlier observations of active processes on Bear Island, it was "easy to go straight to a full understanding of the thing" (Andersson 1906, p. 99).

Today, periglacial regions are identified as those nonglacial parts of the world subject not only to cold-climate conditions but also in particular to intense frost action and repeated ground freezing and thawing (Washburn 1980, French 2017b). Periglacial environments are characterized by either perennially or deep seasonally frozen ground. If sufficiently cold that the ground remains at or below 0°C for two consecutive years or more, the ground becomes perennially frozen, hence permafrost. Permafrost is not a prerequisite for a periglacial environment, as some environments that experience seasonally frozen ground are considered periglacial (French 2017b, Wolfe et al. 2018). It is reasonable to deduce, however, that if permafrost exists in a landscape, it is periglacial,





(Caption appears on following page)



**Figure 2** (Figure appears on preceding page)

(*a*) Lidar-derived slope map from 1-m digital elevation model (US Geological Survey 3DEP) for Chestnut Ridge, eastern Pennsylvania, ~15 km south of the Last Glacial Maximum ice margin. Note ubiquitous relict solifluction lobes on the south-facing slope and the sand quarry at the middle left of the ridge. (*b*) Excerpt from US Geological Survey 7.5' topographic map for the same area as panel *a*. (*c*) Orthoimage (2019) acquired by Pennsylvania Emergency Management Agency for the same area as panels *a* and *b*, showing a new road excavated in 2019 along which periglacial features and deposits were studied (Hertzler 2020; Merritts et al. 2020; Ruck 2020; D. Merritts, J. Marshall, R. Walter, M. Demitroff, N. Hertzler, et al., unpublished article).

and if permafrost existed at some time in the past, the landscape was periglacial at that time. A plausible empirical estimate of a maximum mean annual air temperature (MAAT) for periglacial conditions is about +3°C (French 2017b).

### Periglacial Processes and Features

Investigations of active and formerly periglacial landscapes worldwide over the past ~120 years reveal numerous landforms and deposits indicative of cold-climate conditions and processes. Several groups of general processes are common among all periglacial environments (**Table 1**): ground cooling and freezing, ground warming and thawing, and recurrent freeze-thaw (Murton 2021a). They produce features and deposits that can vary in detail from one place to another, however, because of local differences in cold-climate conditions (e.g., annual temperature amplitudes and snow cover), as with modern contrasts between dry Antarctic terrain and wet Alaskan coastal regions.

The effects of periglacial processes in a given landscape also depend upon the amount and type of ice that accumulates in the ground during cold periods. Ground ice refers to all types of ice contained in frozen (or freezing) ground. Examples span many scales, from thin needles of ice in pores of silty sediment to larger horizontal ice lenses of segregation ice to massive, vertical ice wedges within thermal contraction cracks that can be many meters in depth. Differences in lithology also contribute to variations in periglacial features. Unconsolidated sediments and sedimentary rocks that are fine grained are generally more frost susceptible than other Earth materials (Murton et al. 2000, Murton & Ballantyne 2017).

Common relict periglacial features and their paleoenvironmental implications, per modern analogs, indicate that some are usually associated with former permafrost and extreme cold conditions (Ballantyne 2018) (**Table 2**). These features include frost (thermal contraction) polygons, ice-wedge pseudomorphs (or casts), composite-wedge pseudomorphs, large relict sand wedges, pingo scars, thermokarst involutions, retrogressive thaw slumps, large cryoturbations, active layer failures, talus rock glaciers, and water tracks. Other relict features, such as blockfields and solifluction sheets and lobes, are not diagnostic of former permafrost but are strongly associated with frost weathering and freeze-thaw processes and commonly develop where permafrost exists.

### Polygenetic Periglacial Landscapes

About a century after the publications of Andersson (1906) and von Łozinski (1909), French (2000, 2016) and French & Thorn (2006) asserted that no modern counterpart to von Łozinski's so-called periglacial realm exists today. One reason for their assertion is that few modern periglacial environments in high latitudes of the Northern Hemisphere are as arid and windy as mid-latitude landscapes might have been during Pleistocene cold conditions, when strong katabatic winds flowed off continental ice sheets (French 2000, 2017a). Furthermore, unglaciated





(Caption appears on following page)



**Figure 3** (Figure appears on preceding page)

- (a) Solifluction lobes in a semiarid polar continental climate, Ulu Peninsula, Antarctica. Photograph courtesy of Bethan Davies.  
 (b) Distal end of stone-banked solifluction lobes in Svalbard, Norway. Photograph courtesy of Heginbottom et al. (2012) and USGS.

landscapes that experienced cold-climate conditions during the Pleistocene also have experienced warm-climate conditions during alternating warm intervals of the Quaternary Period. Nevertheless, multiple lines of evidence indicate that periglacial conditions similar to those that resulted in von Łoziński's periglacial facies existed in mid-latitude areas beyond the extent of continental ice sheets during Pleistocene cold conditions.

Murton (2021b) agreed that characteristic periglacial landscapes fully adjusted to Holocene climate conditions are rare today, even though periglacial conditions exist for about 20% of Earth's land surface at present. Murton (2021b) proposed instead that polygenetic periglacial landscapes are more common in both present and past permafrost regions. These landscapes have inherited ancient land surfaces upon which a range of superimposed periglacial landforms might have formed and been preserved, fully or partially, over long timescales ( $>10^4$ – $10^7$  years). Some 51 cold stages identified from the marine isotope record for the past 2.58 Ma (Head 2019) have provided ample opportunity and time for varying degrees of periglaciation at mid-latitudes.

The MAR landscape fits Murton's (2021b) concept of a polygenetic landscape, with its strong signature of multiple embedded geomorphic legacies produced by recurrent cold and warm conditions over glacial-interglacial timescales. The region has many similarities to polygenetic periglacial landscapes in southern England and northwest France (Murton 2021b). All are underlain mostly by Phanerozoic sedimentary rocks on which downslope regolith transport by diffusional processes has smoothed slopes into dominantly convexo-concave shapes with eroding summits and aggrading footslopes (Kirkby 1995) (see **Figures 2** and **3**).

Low relief and gentle hillslope gradients of the MAR have been conducive to widespread preservation of slope features and deposits that sometimes mantle entire hillslopes and even adjacent valley bottoms with up to tens of meters of colluvium (Denny 1951, 1956; Ciolkosz et al. 1986a,b; Braun 1989; Braun et al. 1994; Newell et al. 1989, 2000; Pazzaglia & Cleaves 1998; Newell 2005; Newell & DeJong 2011). Indeed, there is growing recognition that coarse-grained, often angular sediments buried beneath Holocene wetland soils in MAR valley bottoms were colluvial rather than fluvial in origin (Walter & Merritts 2008; Merritts et al. 2011, 2013, 2015; Bodek et al. 2021).

**Table 1 Three general types of periglacial processes produce and shape landforms**

General process	Specific process (with example features)
1. Ground cooling and freezing	a. Thermal contraction and cracking of the ground (polygon networks and near-vertical cracks with ice, windblown sand, or composite of the two) b. Ice segregation, heave, and frost cracking parallel to the ground surface (brecciated rock)
2. Ground warming and thawing	a. Thermal expansion b. Mass movement (solifluction, active layer detachment, retrogressive thaw slump) c. Thaw consolidation and ground settling
3. Recurrent freeze-thaw	a. Cryoturbation (involutions) b. Solifluction (including frost creep and gelifluction)



**Table 2** Paleoenvironmental implications for relict periglacial features

Relict feature(s)	Paleoenvironmental implication(s) for frozen ground	Paleoenvironmental implication(s) for climate conditions
Frost polygons and ice-wedge pseudomorphs (or casts)	Usually CPF DPF in fine sediments	MAAT $\leq -4^{\circ}\text{C}$ in fine sediments MAAT $\leq -8^{\circ}\text{C}$ to $-6^{\circ}\text{C}$ in coarse sediments Rapid winter cooling Temperature of coldest month $\leq -20^{\circ}\text{C}$
Large relict sand and composite wedges	Usually CPF DPF in fine sediments	MAAT $\leq -4^{\circ}\text{C}$ in fine sediments MAAT $\leq -8^{\circ}\text{C}$ to $-6^{\circ}\text{C}$ in coarse sediments Rapid winter cooling Temperature of coldest month $\leq -20^{\circ}\text{C}$ Eolian sand infill implies unvegetated source and strong winds Might indicate aridity
Seasonal frost cracks and soil wedges	Deep seasonal ground freezing	MAAT $\leq 0^{\circ}\text{C}$ Rapid winter cooling
Pingo scars	Hydrostatic pingos: CPF and site of former lake Hydraulic pingos: CPF or DPF	MAAT $\leq -6^{\circ}\text{C}$ to $-4^{\circ}\text{C}$ MAAT $\leq -3^{\circ}\text{C}$
Thermokarst involutions	Thaw of ice-rich permafrost	MAAT $\geq -4^{\circ}\text{C}$
Retrogressive thaw slumps	Ice-rich CPF, possibly DPF	MAAT $-1^{\circ}\text{C}$ to $-6^{\circ}\text{C}$ if DPF, $< -5^{\circ}\text{C}$ to $-8^{\circ}\text{C}$ if CPF
Large cryoturbations ( $\geq 0.6\text{-m}$ amplitude)	Former active layer above permafrost May indicate former minimum active-layer depth If $\geq 0.6\text{-m}$ amplitude, likely CPF	MAAT $-1^{\circ}\text{C}$ to $-6^{\circ}\text{C}$ if DPF, $< -5^{\circ}\text{C}$ to $-8^{\circ}\text{C}$ if CPF
Autochthonous blockfields	Predominantly mechanical (frost) weathering Possibly indicate depth of former active layer	Not available
Solifluction sheets and lobes	Seasonal freeze-thaw of soil, in both permafrost and nonpermafrost environments	Not available
Granular gelifluctate (head)	Seasonal freeze-thaw of soil, in both permafrost and nonpermafrost environments	Not available
Active-layer failures	Ice-rich permafrost	MAAT $-1^{\circ}\text{C}$ to $-6^{\circ}\text{C}$ if DPF, $< -5^{\circ}\text{C}$ to $-8^{\circ}\text{C}$ if CPF
Talus rock glaciers	Permafrost; MAAT $< -2^{\circ}\text{C}$	High debris input
Water tracks	Permafrost	MAAT $-1^{\circ}\text{C}$ to $-6^{\circ}\text{C}$ if DPF, $< -5^{\circ}\text{C}$ to $-8^{\circ}\text{C}$ if CPF

Table modified from Ballantyne (2018), table 16.1. Abbreviations: CPF, continuous permafrost; DPF, discontinuous permafrost; MAAT, mean annual air temperature.

## PLEISTOCENE COLD CONDITIONS, GEOLOGIC SETTING, AND PERIGLACIATION

### Pleistocene Cold Conditions

Most of the MAR has a humid continental (subtropical to the south) climate at present, with MAAT ranging from  $\sim 8$  to  $14^{\circ}\text{C}$  from northern Pennsylvania to southern Virginia, respectively.



During repeated North American ice sheet advances of the Pleistocene Epoch [ $\sim$ 2.6 million to 11.7 thousand years ago (Batchelor et al. 2019)], cold conditions extended beyond proglacial margins, ultimately placing broad areas into the periglacial domain (Péwé 1983, French 2017b). The most recent of these periods of ice sheet growth is referred to as the Wisconsin. Although mapped terminal positions of former ice sheets vary locally, in general they are similar to that of the LGM in the MAR (Braun 2004, 2011). Wisconsin glaciation in North America occurred primarily during marine oxygen isotope stages (MIS) 4 through 2 ( $\sim$ 71 to 11.7 ka, respectively). The Wisconsin is further subdivided into early (MIS 4,  $\sim$ 71–57 ka), middle (MIS 3,  $\sim$ 57–28 ka), and late (MIS 2,  $\sim$ 28–11.7 ka BP) periods/stages. The late Pleistocene Epoch encompasses all of these and MIS 5, from  $\sim$ 130 to 11.7 ka BP. It is acknowledged that some prefer to correlate the Last Interglacial with MIS 5e alone, rather than the entire MIS 5. In such a correlation, the Early Wisconsin would also include MIS 5d to 5a, starting at  $\sim$ 115 ka (Otvos 2015).

Based on downscaled monthly temperature data from the Coupled Model Intercomparison Project (CMIP5)/Paleoclimate Modelling Intercomparison Project (PMIP3) ensemble-averaged climate simulations for the LGM ( $\sim$ 21 ka), the MAR had a MAAT range from about  $-12^{\circ}\text{C}$  near the ice sheet margin to  $\sim 0^{\circ}\text{C}$  in what is now Virginia,  $\sim$ 14 to  $20^{\circ}\text{C}$  cooler than modern MAATs in the region (Marshall et al. 2021, Shafer et al. 2021). These paleotemperature estimates overlap the range of temperature conditions for periglacial conditions and permafrost occurrence.

Paleovegetation studies from pollen and macrofossils at several sites in the MAR are consistent with the reconstructed MAAT, at least several degrees cooler than at present during the middle Wisconsin and  $\sim$ 6– $12^{\circ}\text{C}$  cooler during the Late Wisconsin (Watts 1979, Delcourt & Delcourt 1981, Kneller & Peteet 1999, Eaton et al. 2003a, Whittecar et al. 2007). Boreal forests and herbaceous tundra have been documented from pollen and macrofossils that date to  $\sim$ MIS 4 through MIS 2 in much of the MAR (Martin 1958, Maxwell & Davis 1972, Watts 1979, Whittecar et al. 2007). Close to the ice margin, central Appalachian highlands had tundra vegetation and cold, arid, windy conditions until  $\sim$ 12,500 years BP (Watts 1979, Peteet et al. 2012).

The longest duration record of paleovegetation change is from an  $\sim$ 25-m sediment core from Hybla Valley, eastern Virginia. Here, Litwin et al. (2013) documented frequent, strong paleovegetation shifts during the past  $\sim$ 130 ky based on radiocarbon and optically stimulated luminescence (OSL) dating and high-resolution analysis of fossil pollen. Dominantly arboreal local vegetation alternated from high boreal (cold period) to subtropical (warm period) forests. The Hybla Valley pollen record indicates abrupt episodes of warming and cooling multiple times during the  $\sim$ 100,000 years prior to the LGM.

## Geologic and Topographic Setting

Rock type, degree of rock fracturing, elevation, relief, and other factors strongly influence periglacial processes and resultant landforms. Elevations of mountain peaks and plateaus in the MAR range from several hundred to  $\sim$ 1,500 m, with local relief up to  $\sim$ 600 m. Most slopes are less than  $15^{\circ}$  but in places along ridge crests are near vertical. The MAR Valley and Ridge (MARVAR) physiographic province of the Appalachian Mountains, where the most prominent periglacial slope features are observed, consists of thick packages of folded and faulted Paleozoic sedimentary rocks with significant contrasts in rock erodibility. Northeast-southwest trending, broad plunging folds and long-term erosion of rocks within these structures have resulted in prominent, linear ridges of resistant caprocks (typically orthoquartzites, sandstones, and sometimes conglomerates) adjacent to elongate valleys underlain by less resistant rocks, primarily shales and carbonates. Shales generally form low hills between sandstone ridges and limestone or dolomite valleys. Orthogonal fracture sets result in highly jointed rocks throughout the region.



and, in combination with variations in bedding thickness, yield a range of clast sizes from rock weathering, typically cobble to boulder sized from sandstones and gravel sized from shales.

A general view of the MAR's landscape history is one of low erosion rates, intense chemical weathering, and saprolite formation on crystalline rocks (primarily in the Piedmont) from Late Cretaceous to late Miocene time, followed by post-Miocene fluvial incision and increased erosion rates, in turn followed by Quaternary periglaciation and colluviation (Costa & Cleaves 1984). Quaternary geologic erosion rates are low and regolith residence times correspondingly long (Hancock & Kirwan 2007; Portenga & Bierman 2011; Miller et al. 2013; Portenga et al. 2013, 2019; West et al. 2013, 2014; Duxbury et al. 2015; Del Vecchio et al. 2018). Erosion rates derived from  $^{10}\text{Be}$  range from 3 to 50 m My $^{-1}$ , but most are  $\sim$ 10–20 m My $^{-1}$  (see compilation in Del Vecchio 2021, Del Vecchio et al. 2021). Possibly higher erosion rates from south to north have been attributed to greater frost weathering (Portenga et al. 2019). Given the duration of climate shifts, typically tens of thousands of years, and generally low long-term erosion rates, the geomorphic record of climate change is relatively well preserved, albeit with interpretative challenges from its polygenetic aspects, dense vegetation cover at present, and scarce exposures of the subsurface (cf. Newell 2005, Newell & DeJong 2011).

### Overview of Mid-Atlantic Region Periglaciation: Blockfields, Patterned Ground, Frost Wedges, and Rubble Slope Deposits

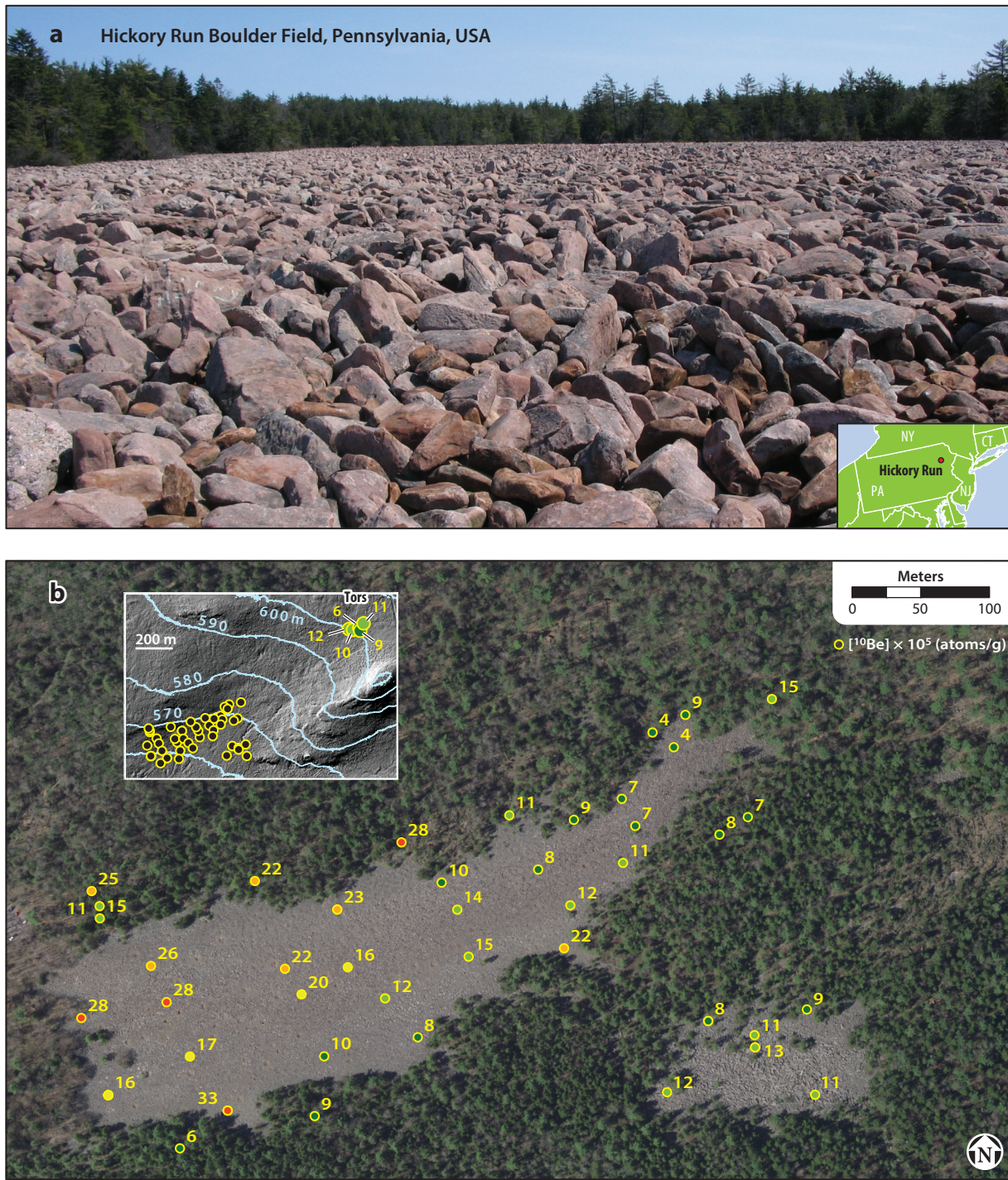
Evidence of periglaciation has been reported from the southernmost extent of the glaciated parts of Pennsylvania, New Jersey, and Delaware to the wholly unglaciated states of Maryland, West Virginia, and Virginia to farther south at higher elevations (see **Figure 1a**). Limited by relatively dense vegetation cover and scarcity of ephemeral outcrops, early workers focused on the surficial aspects of barren block deposits and patterned ground [e.g., sorted stripes (Clark 1968)] and exposures in quarries. Just as the attention of von Łoziński (1909), Andersson (1906), and others was drawn to what appeared to be inactive rubble drifts that mantled hillslopes and some valley bottoms throughout Europe and elsewhere, early geologists in the inland MAR concentrated on striking expanses of what came to be called blockslopes on hillslopes (up to 35°) and blockstreams on valley bottoms (Potter & Moss 1968, Moss 1976, Clark & Ciolkosz 1988, Nelson et al. 2007, Ballantyne 2018) (**Figure 4a**). Growing literature on blockfields worldwide indicates that all of those on valley bottoms, the blockstreams, are “...manifestly relict, and...occur outside the limits of Late Pleistocene glaciation” (Ballantyne 2018), as is the case for the Hickory Run boulder field (HRBF).

Three aspects of blockfields were particularly intriguing to early investigators in the MAR: the size of the clasts, with some boulders up to 10 m in length; the downslope distance that boulders traveled from source rocks, up to several kilometers (Ciolkosz et al. 1986a,b; 1990); and the challenge in identifying a process that could move coarse sediment such long distances, sometimes over slopes of only a few degrees. Determining the origin of these features took decades of investigation and is still being resolved for blockfields worldwide (Goodfellow 2012, Ballantyne 2018). Determining their age of formation has been equally challenging, but cosmogenic isotope dating techniques provide new means of age control (Denn et al. 2017).

A well-known example is the HRBF in eastern Pennsylvania (Smith 1953, Sevon 1987), the first blockstream in the MAR for which multiple cosmogenic isotopes were used to evaluate exposure history (Denn et al. 2017) (see the sidebar titled Case Study of the Hickory Run Boulder Field, Pennsylvania, and Similarities to Falkland Island Stone Runs). This study confirmed that the HRBF is long-lived and highly resistant to further weathering.

Nelson et al. (2007) showed that 96 relict blockfields within 11 locales in the MAR are generally found at higher elevations (increasing from several hundred to greater than 800 m) with distance





(Caption appears on following page)



**Figure 4** (Figure appears on preceding page)

(a) Hickory Run Boulder Field, eastern Pennsylvania, ~2 km south of the Last Glacial Maximum ice sheet boundary. It is the largest boulder field in North America and a National Natural Landmark. Photo courtesy of Martin Helmke. (b)  $^{10}\text{Be}$  concentration of boulders and tors at Hickory Run. The inset shows the locations of tors relative to the main boulder field (*upper left*). Note the generally positive correlation between  $^{10}\text{Be}$  concentration and downslope distance. Figure adapted from Denn et al. (2017).

along an ~800-km transect southward from the LGM ice margin, possibly indicating an association with permafrost conditions. Using modern climate data for Appalachian lapse rates and published temperature departures for LGM climate conditions, Nelson et al. (2007) concluded that all but one blockfield site was above timberline during the LGM and formed under MAATs between  $-1.2$  and  $-4.0^\circ\text{C}$ , conditions conducive to permafrost.

Since the mid-twentieth century, geologists have described many periglacial features and deposits other than blockfields throughout the MAR, including patterned ground, frost wedges, mantles of matrix-supported angular rubble along entire hillslopes, lobes and benches of boulder-rich sandstone colluvium, and slope-stratified deposits of thinly bedded shale-chip colluvium (Peltier 1949, 1950; Denny 1951, 1956; Potter & Moss 1968; Mills 1981; Péwé 1983; Carter & Ciolkosz 1986; Kite 1987; Clark & Ciolkosz 1988; Braun 1989, 1996; Gardner et al. 1991;

### CASE STUDY OF THE HICKORY RUN BOULDER FIELD, PENNSYLVANIA, AND SIMILARITIES TO FALKLAND ISLAND STONE RUNS

The nearly flat Hickory Run Boulder Field (HRBF) at an elevation of ~500 m in east-central Pennsylvania is the largest boulder field (~150 m wide by 550 m long) in North America (Sevon & Braun 2000) (see **Figure 4a**). Located along the axis of a small valley ~2 km south of the Last Glacial Maximum ice sheet boundary, this largely barren field of openwork (no matrix) boulders is at least several meters thick (Smith 1953). Sandstone and conglomeratic boulders sourced from nearby ridgelines are up to 10 m in length yet somehow were loosened from source rocks and moved downslope along a  $1^\circ$  gradient. The HRBF appears inactive under modern climatic conditions. Explanations of its origins generally include frost weathering to produce rubble from jointed source rocks and downslope transport by slow mass movement, possibly solifluction. If so, then some process winnowed fines from the original matrix after deposition, as solifluction usually requires a fine-grained matrix to hold moisture for mass movement.

The HRBF demonstrates three common challenges in periglacial studies: whether a relict feature might be periglacial, if it formed in association with permafrost, and when it formed, similar to questions pondered by Andersson (1906) in the Falkland Islands. Recent age control adds further information for the HRBF, but also complexity, and does not confirm a periglacial origin (Denn et al. 2017). Results from *in situ* cosmogenic  $^{10}\text{Be}$  and  $^{26}\text{Al}$  of 52 samples taken from the surfaces of boulders along the length of the field indicate that boulders have near-surface exposure histories that span 70 to 600 ky, persisting through multiple glacial-interglacial cycles (see **Figure 4b**). A positive correlation between  $^{10}\text{Be}$  concentration and downslope distance along the boulder field is consistent with slow movement of a stable, persistent landform but not specific timing of boulder movement (Denn et al. 2017). Similar cosmogenic results were obtained by Wilson et al. (2008) for boulder streams in the Falkland Islands, where near-surface exposure histories of boulders span 42 to 730 ky.

Based on current understanding of the HRBF and other blockfields in the mid-Atlantic region, nothing about them is diagnostic of the former presence of permafrost, and yet most researchers attribute their origin to periglacial conditions and processes. The main reasons are that blockfields are inactive under modern climatic conditions and no modern geomorphic processes produce such copious amounts of large boulders or transport them on low-gradient slopes.



Middlekauff 1991; Snyder & Bryant 1992; Braun et al. 1994; Marsh 1998, 1999; Pazzaglia & Cleaves 1998; French 2000; Eaton et al. 2003a; Pazzaglia et al. 2006; Nelson et al. 2007; Grote & Kite 2010; Newell & DeJong 2011; Merritts et al. 2014, 2015, 2020; Grote 2017; Del Vecchio et al. 2018; Del Vecchio 2021). Thermal contraction polygons are highly common on some shale hillslopes in New Jersey (Walters 1978) and Pennsylvania (Merritts et al. 2015, 2020; D. Merritts, J. Marshall, R. Walter, M. Demitroff, N. Hertzler, et al., unpublished article). Relict water tracks, similar in morphology to those active in Antarctica and other cold regions (Levy et al. 2013) with permafrost today, are abundant on the same hillslopes in Pennsylvania (Merritts et al. 2015, 2020; D. Merritts, J. Marshall, R. Walter, M. Demitroff, N. Hertzler, et al., unpublished article).

These various periglacial features and deposits are described in more detail below. Notably, evidence of valley, cirque, or rock glaciers has not been documented in the region, although such features are common in some periglacial environments with permafrost. Pingos are considered diagnostic of past permafrost, but no relict pingo scars have been identified with certainty in the MAR (Marsh 1987, 1999).

## PERMAFROST AND ITS FORMER EXTENT

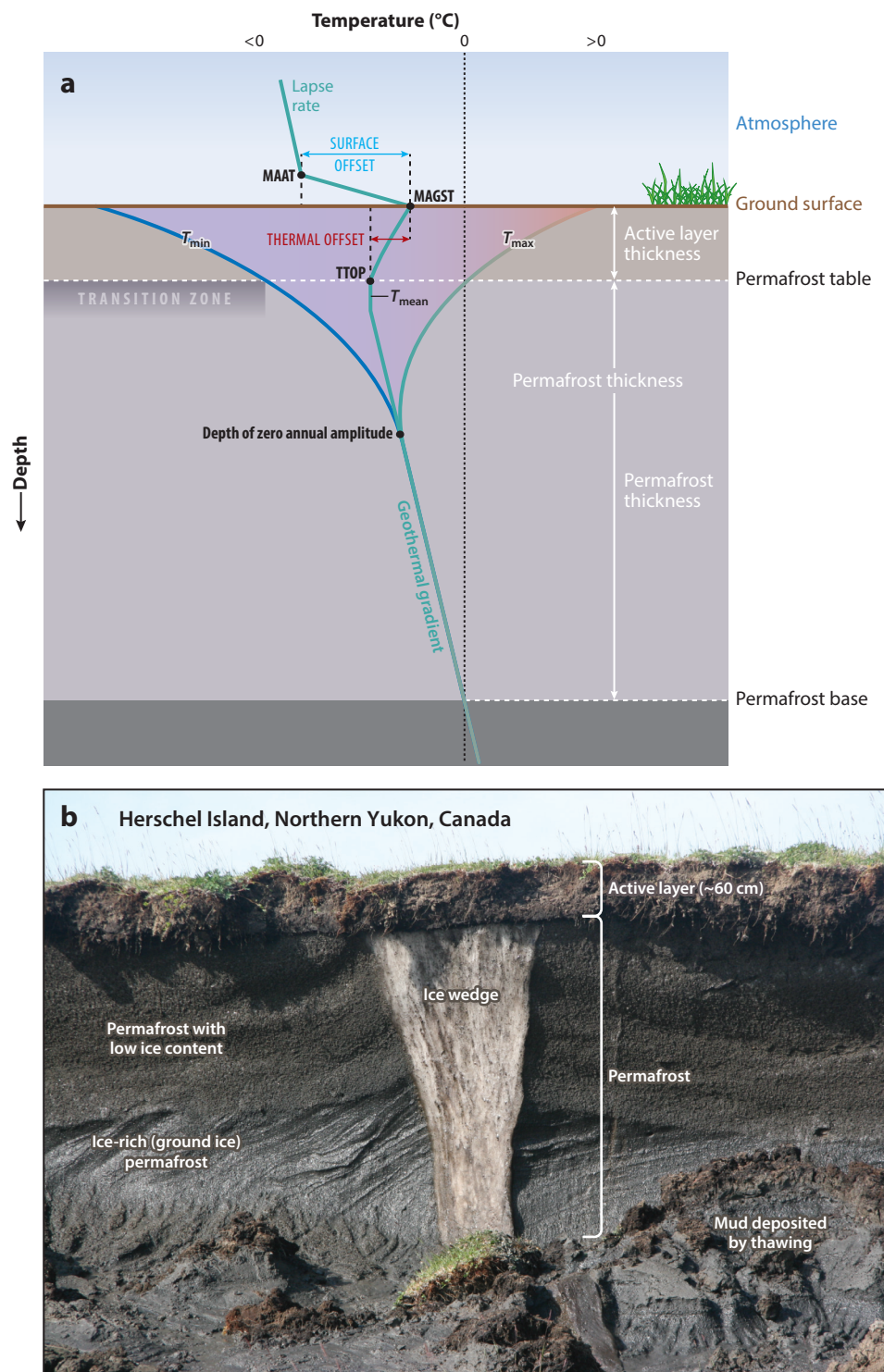
The existence of permafrost significantly influences periglacial processes. Frost weathering, for example, is generally deeper and more intense in permafrost regions than areas with seasonally frozen ground (Murton et al. 2006). Mass movement is more common where permafrost exists due to the potential for excess ice that exceeds porosity of the host material. Melt of excess ice can lead to liquefaction and thaw consolidation of material above perennially frozen ground during thaw (see **Tables 1** and **2**). Here we examine modern permafrost and its distribution as a prelude to mapping its former extent in the MAR.

### Permafrost Distribution and Structure

Permafrost is perennially frozen ground that remains at or below 0°C for two or more consecutive years (French 2007), with an uppermost active layer (typically less than or equal to 0.5 m thick) that thaws seasonally (**Figure 5**). Within the Northern Hemisphere, about 24% of exposed land area is underlain by permafrost, mostly above the latitude of 60°N. Permafrost generally thins to the south in the Northern Hemisphere, varying from thick and continuous to thinner and discontinuous and eventually sporadic before disappearing completely (**Figure 6**). The active layer correspondingly thickens toward the equator. Where spatial coverage of permafrost is greater than 90% in a given region, it is designated as continuous (Ballantyne 2018). Where permafrost covers ~50–90% of the area, it is designated as discontinuous. Sporadic permafrost describes a spatial coverage of 10–50%, and isolated permafrost a coverage of less than 10%. In general, continuous permafrost occurs today in regions with MAAT less than approximately –6 to –8°C, and discontinuous permafrost in regions with MAAT less than approximately –0.5 to –2°C (Péwé & Brown 1973, Gruber 2012). In continuous permafrost regions, ice-rich sediment at the base of the active layer, the transient layer, commonly marks the boundary with the top of permafrost, the permafrost table. Moisture migration to this transition zone in response to thermal gradients leads to growth of segregated ice lenses.

Permafrost that does not exist at present is referred to as past permafrost (French 2008, French & Millar 2014). During cold glacial periods, permafrost advanced toward equatorial regions, as did ice sheets. Up to ~21–26% more area of the Northern Hemisphere had permafrost during the LGM than at present (Vandenbergh et al. 2014, Lindgren et al. 2016). The maximum permafrost extent, the Last Permafrost Maximum (LPM), is estimated to have occurred ~25–17 ka,





(Caption appears on following page)



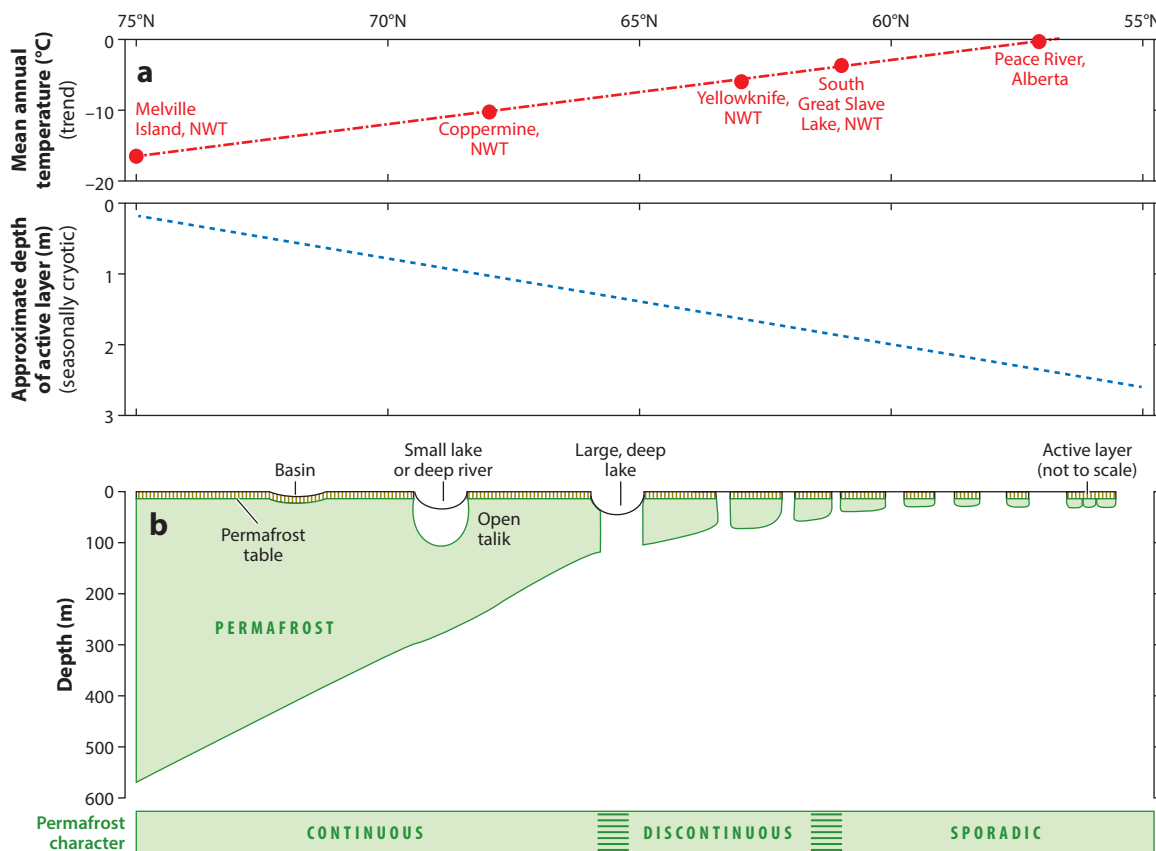
**Figure 5** (Figure appears on preceding page)

(a) Equilibrium thermal regime of ground and near-surface atmosphere in permafrost terrain.  $T_{\text{mean}}$  is the mean annual ground temperature. The base of the active layer (also permafrost table) is at  $0^{\circ}$  isotherm.  $T_{\text{min}}$  is the minimum annual ground temperature.  $T_{\text{max}}$  is the maximum annual ground temperature.  $T_{\text{mean}}$  declines toward the TTOP. The shaded envelope between the ground surface and depth of zero annual amplitude is the temperature range between  $T_{\text{min}}$  and  $T_{\text{max}}$ . Panel adapted from Murton (2021a). (b) Photo taken on Herschel Island in the Yukon showing an ice wedge that extends ~5 m below the active layer ( $69^{\circ}34'13.5''\text{N}$ ;  $139^{\circ}01'03.9''\text{W}$ ). The top of the ice wedge corresponds to the base of the active layer. Photo courtesy of Wayne Pollard. Abbreviations: MAAT, mean annual air temperature; MAGST, mean annual ground surface temperature; TTOP, temperature at top of permafrost.

but its timing is not necessarily coincident with that of the LGM or the same age throughout the Northern Hemisphere (Vandenbergh et al. 2014).

### Mapping Relict Periglacial Features and Past Permafrost Extent

As the field of periglacial geomorphology developed in the twentieth century, the overwhelming importance of permafrost and related processes became clear (French 1979, 2003). Murton (2021b) noted that permafrost areas are more readily identified than those that are seasonally

**Figure 6**

Generalized latitudinal distribution of permafrost characteristics showing (a) increase in mean annual air temperature, (b) increase in depth to base of active layer, and decrease in permafrost thickness with distance from high to low latitudes. Note transitions from continuous to discontinuous and sporadic permafrost. Abbreviation: NWT, Northwest Territories. Figure adapted from Heginbottom et al. (2012).



frozen and suggests that mapping the maximum extent of former permafrost is likely to approximate the region of recurrent, persistent permafrost associated with cyclical cold periods (Murton 2021b). The challenge, however, is that few landforms are uniquely diagnostic of the occurrence of permafrost or recurrent freeze-thaw (Ballantyne & Harris 1994, Ballantyne 2018) (see **Table 2**). In addition, relict periglacial features vary in potential for preservation, often obscured by modern vegetation and commonly buried by more recent deposits, some of which might have formed during times of deep seasonal freezing in the wake of permafrost thaw (i.e., polygenetic periglacial landscapes). Lastly, in response to warming and permafrost thaw, mass movement can become widespread, as water released during ground thawing cannot easily infiltrate the hard permafrost substrate (Gooseff et al. 2009). In essence, permafrost formation periods were likely to have been bracketed by episodes of deep seasonal freezing and ended with thaw-related geomorphic processes that modified or even destroyed evidence of former permafrost (Kirkby 1995, French et al. 2009).

Despite incomplete preservation and other issues, numerous geomorphic and sedimentary features associated with former permafrost have been mapped south of the maximum extent of continental glaciation in the MAR (Péwé 1983, French & Millar 2014) (see **Figure 1a**). Péwé (1983) compiled features considered to be of likely Wisconsin age, carefully documenting sources of information for each. French & Millar (2014) updated Péwé's synthesis of periglacial features, focusing in particular on the possible extent of past permafrost associated with the time of the LGM (see **Figure 1a**).

Periglacial features included in both Péwé's (1983) and French & Millar's (2014) maps (see **Figure 1a**) are as follows: more than 250 frost wedges and associated networks of thermal contraction cracking polygons at several sites within 10 to 45 km of the ice sheet margin in northern New Jersey (Walters 1978; portrayed as three triangles by Péwé 1983 and French & Millar 2014); solifluction deposits and other colluvia mapped in northern Pennsylvania near the Wisconsin ice sheet terminus (Denny 1956) and much farther south in North and South Carolina, with a large gap between the sites; and rock streams, block streams, blockfields, talus, rubble sheets, and patterned ground phenomena (e.g., sorted stone stripes and circles) throughout the region.

Based on this compilation, Péwé (1983) mapped a speculative Wisconsin permafrost limit that covered only parts of Pennsylvania and New Jersey, with the exception of a prong of possible permafrost extending southward along higher elevations of the Appalachian Mountains. The map presented by French & Millar (2014) is derived from Péwé's (1983) map, with no new features included on the map for the MAR. Based on a "critical evaluation" of the references used by Péwé (1983) and analysis of new work on periglacial features published since 1983, French & Millar (2014, p. 669) extended the speculative limit of permafrost much farther to the south. French & Millar's (2014) mapping of possible LGM past permafrost encompasses all of nonglaciated Pennsylvania and New Jersey, all of Delaware and Maryland, much of West Virginia and Virginia, parts of North and South Carolina, and a small portion of northeastern Georgia. Their mapping extends the zone of possible permafrost by hundreds of kilometers in comparison to Péwé's (1983) mapping.

All other relict periglacial features included in the compilations of Péwé (1983) and French & Millar (2014) are considered to be possible, not conclusive, indicators of permafrost that provide supporting information of cold-climate conditions with frost action. French & Millar's (2014, p. 668) commentary on the topic is relevant to this review:

...the use of solifluction and associated phenomena such as colluvium, cryoturbated sediments, and frost-shattered bedrock, although certainly evidence for intense frost action, are not convincing proof of perennial frost...differentiation between seasonal and perennial frost is the "Achilles' heel" (French 2011) of any attempt to map the extent of permafrost, both today and in the past.



## RElict PERIGLACIAL FEATURES DIAGNOSTIC OF PAST PERMAFROST

Relict periglacial features widely regarded as diagnostic of past permafrost are thermal contraction cracking features that include polygons and their underlying ice-wedge casts (or pseudomorphs) and relict sand wedges, but generally only for wedges greater than ~2 m in depth (Black 1976, Murton et al. 2000, French 2007, Vandenberghe et al. 2014) (see **Table 2**). Smaller frost wedges are associated with deep seasonal freezing. Here we describe active thermal contraction crack polygons and ice and sand wedges and then turn to relict features identified in the MAR.

### **Polygons and Wedges Formed by Thermal Contraction Cracking**

Plan-view networks of polygons and associated wedges formed by thermal contraction cracking are the most common periglacial features in lowland regions of continuous and sometimes discontinuous permafrost and occur occasionally in areas of deep seasonal freezing (Mackay 1974, Burn 1990, Mackay & Burn 2002, Christiansen et al. 2016, Wolfe et al. 2018) (see **Table 2**). Cooling leads to thermal contraction and horizontal tensile stresses in near-surface Earth materials. When the tensile strength of the ground is exceeded, a near-vertical crack forms perpendicular to the greatest extensile stress. With time, cracks grow and join to form polygonal networks that resemble mud cracks formed during drying (Lachenbruch 1962, 1966; Plug & Werner 2001, 2008) (**Figure 7**). The cracks can provide accommodation space for near-vertical wedges of sediment and/or ice, referred to in general as frost wedges.

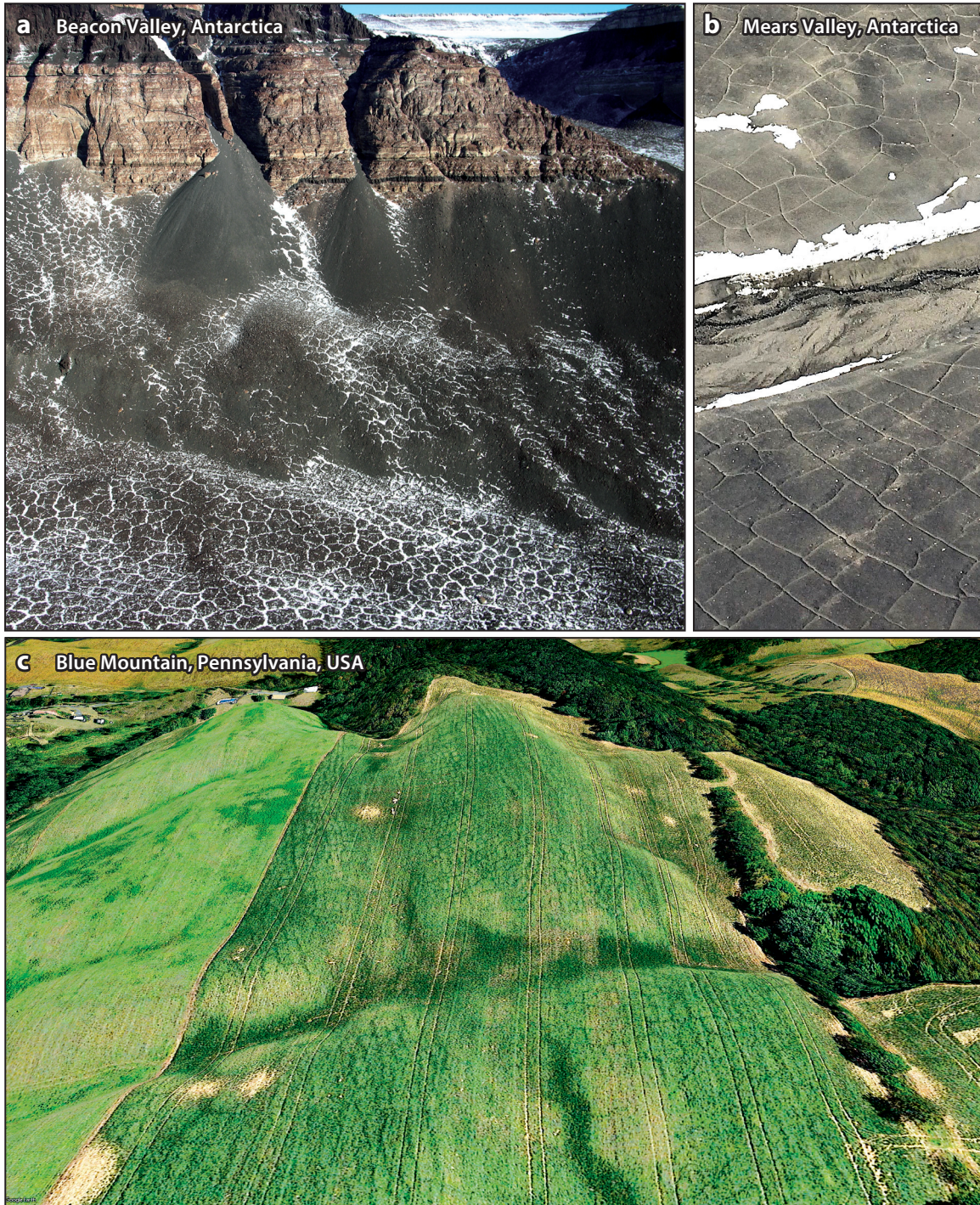
Thermal contraction crack polygons form in frost-susceptible bedrock and unconsolidated sediment, including colluvium (see polygons in debris aprons, **Figure 7a**). Polygon diameters typically range from ~10 m to several tens of meters, and most have orthogonal, random orthogonal, or hexagonal patterns (French 2017b). Variations in polygon patterns and dimensions are associated with spatial variability in moisture and vegetation, and with different coefficients of expansion and contraction that are temperature dependent, among other factors (French 2017b).

Active thermal contraction crack polygons and frost wedges have been studied at numerous cold-climate locations on Earth (Christiansen et al. 2016; summary of sites in French 2017b and Ballantyne 2018) (see **Figure 7a,b**). Modern thermal contraction cracking commonly occurs during extended periods of frozen ground conditions at MAAT of -6 to -8°C or lower (similar to that for continuous permafrost) and ground surface temperatures between -13 and -20°C at the time of cracking (compilation of literature in French 2007 and Ballantyne 2018). Rapidly falling temperatures of 1.8°C/day for many days at a time are conducive to thermal contraction cracking (Mackay 1993). As a consequence, thermal contraction crack polygons and their associated wedges provide nearly unequivocal evidence for the existence of permafrost and large temperature amplitudes (French & Millar 2014, French 2017b). Traces of former thermal contraction crack polygons and relict wedges have been mapped throughout mid-latitude regions in Europe, Asia, and North America (Vandenberghe et al. 2014, Christiansen et al. 2016, French 2017b, Beerten et al. 2021).

### **Ice and Sand Wedges, Ice-Wedge Pseudomorphs, and Relict Sand Wedges**

Studies of modern frost wedges underlying thermal contraction crack polygon networks demonstrate that they are the result of filling of near-vertical thermal contraction cracks with ice, soil, or a composite of the two (Lachenbruch 1962, Murton et al. 2000, Murton 2013, French 2017b). During cold months, cracks occur in permafrost due to thermal contraction and fill with snow, hoarfrost, and water that freezes in contact with the permafrost. Ice wedges grow incrementally wider during successive cycles of cracking and filling. Where moisture and vegetation are scarce,





(Caption appears on following page)



**Figure 7** (Figure appears on preceding page)

(a) Thermal contraction polygons in the Antarctic Dry Valleys (Beacon Valley, 77.8°S, 160.6°E). The periglacial figures are sublimation-type polygons with sand wedges in till (*bottom*) and debris aprons (*middle*). Polygons range from 10 to 40 m in diameter. See Levy et al. (2013). Photo courtesy of Joseph Levy. (b) Thermal contraction crack polygons in the Antarctic Dry Valleys. The sand-wedge polygons in Miers Valley (near 78.1°S, 160.1°E) formed in the Last Glacial Maximum (LGM)-aged ice-cored Ross Sea Drift (glacial and related deposits). The polygons range from 5 to 20 m in diameter. See Levy et al. (2006). Photo courtesy of Joseph Levy. (c) Traces of relict thermal contraction crack polygons with sand-filled boundaries (relict sand wedges) on crests and mid-slope areas of low-relief swales formed in Ordovician Martinsburg Formation shale, southeastern Pennsylvania, ~125 km south of the LGM ice margin (40°15'46.78"N, 77°13'6.44"W; Google Earth imagery September 6, 2013). The site is near Waggoner's Gap, along the southern footslope of Blue Mountain (see **Figure 1a**). The eastward view is using a September 6, 2013, air photo in Google Earth (eye altitude ~600 m). Dark areas are moist, silty, sandy soil, in contrast to drier areas of shale bedrock, with silty sand in swales reworked and redeposited from slopewash. Dark drainage features follow bedrock fractures and resemble water tracks in Antarctica. See Levy et al. (2011).

fine sediment is available, and winds are relatively strong, cracks can fill with aeolian material rather than ice, forming what are called sand wedges, although the infill ranges from silt to sand in size (French 2017b). Where mixtures of ice and sand fill the void formed by cracking, wedges are referred to as composite.

During climate amelioration (warming) and permafrost thaw, frost wedges become relict. The void left where ice formerly existed in a wedge can become filled with secondary material, such as detritus from the walls of the crack and soil and organic matter from above. The relict feature is referred to as an ice-wedge pseudomorph or cast (Murton et al. 2000). The primary infill in sand wedges, in contrast, typically is preserved and the relict feature known as a relict sand wedge. For composite wedges, the relict feature is a composite-wedge cast.

### **Ice-Wedge Pseudomorphs and Relict Sand Wedges in the Mid-Atlantic Region Coastal Plain**

It was the discovery and detailed description of relicts of many thermal contraction cracking features, or a re-evaluation of previously identified ones, in pits and quarries in the MACP (**Table 3** and citations therein) that led French et al. (2009) and French & Millar (2014) to extend the limit of LGM permafrost over a broader region than that of Péwé's (1983) earlier synthesis (see **Figure 1a**). Most of the relict features are considered to be sand or composite wedges (M. Demitroff, personal communication) (**Figures 8 and 9**). Relict sand wedges and composite-wedge pseudomorphs with some age controls have been described in detail at multiple sites in the Coastal Plain of New Jersey (French & Demitroff 2001, 2012; French et al. 2003, 2007, 2009; Demitroff et al. 2008; French 2011; Demitroff 2016) (**Table 3**). All formed during either MIS 2 or 4, with some showing evidence of recurrent cracking during both stages (see **Table 3**). A MAAT of –6 to –8°C at the time of their formation was estimated by French et al. (2009b).

### **Recent Discoveries of Traces of Thermal Contraction Polygon Networks Throughout the Mid-Atlantic Region**

Since the work of French & Millar (2014), two studies have reported significant discoveries of striking traces of thermal contraction polygon networks at hundreds of sites in the MAR, with more likely to exist (Gao 2014; Merritts et al. 2015, 2020; D. Merritts, J. Marshall, R. Walter, M. Demitroff, N. Hertzler, et al., unpublished article) (**Figures 9–11**). Using multiple years and seasons of Google Earth™ imagery, Gao (2014) identified polygon trace remains in unconsolidated Cenozoic sediments throughout higher-elevation parts of the MACP, from near the LGM ice margin in northern New Jersey (~41°N) to Annapolis (~39°N), a distance of about 250 km



**Table 3 Compilation of ice, sand, and composite wedges information, mid-Atlantic region, eastern United States**

General locations(s)	Location(s) or town(s) (Universal Transverse Mercator coordinates)	Feature(s) (evidence)	Feature age (technique)	Feature dimensions	Host material (age, lithology)	Paleoenvironmental implication(s)	Citation(s)
Central New Jersey (Triassic Lowland)	South Bound Brook and Manville, New Jersey (examples at 4486982.00 m N, 537358.00 m E, 4487909.00 m N, 537448.00 m E, in 12/31/2009 USDA Farm Service Agency photos)	Networks of polygonal cracks in shale (air photos and field work by Walters 1978; Google Earth imagery by D. Merritts, J. Marshall, R. Walter, M. Demitroff, N. Hertzler, et al., unpublished article)	Unknown, interpreted as possible LGM	Polygon diameters 3 to >30 m, mean diameter 20 m	Passaic Formation (Triassic, siltstone and shale)	Interpreted as possible PMF (continuous or discontinuous)	Walters 1978; D. Merritts, J. Marshall, R. Walter, M. Demitroff, N. Hertzler, et al., unpublished article
Central New Jersey (Triassic Lowland)	Multiple sites near South Bound Brook and Manville, New Jersey	Relict sand wedges or possibly composite-wedge pseudomorphs (>200; field work, excavations)	Unknown, interpreted as possible LGM	Wedge east depths 0.25 to 2.6 m; mean depth 1.25 m, widths 0.1 to 2.4 m; mean width 0.5 m	Passaic Formation (Triassic, siltstone and shale)	Interpreted as possible PMF (continuous or discontinuous)	Walters 1978
Central New Jersey, Pine Barrens	Coyle Airfield (4407783.00 m N, 549476.00 m E)	Relict sand wedges (open pit)	Late Pleistocene (OSL)	Wedge east depths 1.5 to 2.4 m; widths 0.1 to 0.3 m	Coastal Plain sediments (Neogene, unconsolidated fluvial and marginal marine sediments)	≥ MIS-4 PMF	French et al. 2007, Demitroff 2016
Southern New Jersey, Pine Barrens	Unexpected pit, Newtonville (39.570200 N, 74.910700 W)	Relict sand wedges and ground-wedge casts* (open pit)	Late Pleistocene (OSL)	Wedge east depths 0.5 to 2.7 m; widths 0.1 to 0.3 m (MIS-2 to 0.5 m)	Coastal Plain sediments (Neogene, unconsolidated fluvial and marginal marine sediments)	LGM and ≥ MIS-4, PMF and DSF	French et al. 2003, 2005, 2007; Demitroff 2016
Southern New Jersey, Pine Barrens	Dorchester pit, Port Elizabeth (43°49'41.50 m N, 50°44'23.00 m E)	Relict sand wedges and ground-wedge casts (sand and gravel pit)	Late Pleistocene (OSL)	Wedge depths 0.5 to 2.7 m; widths 0.1 to 0.3 m (MIS-2 to 0.5 m)	Coastal Plain sediments (Neogene, unconsolidated fluvial and marginal marine sediments)	LGM and ≥ MIS-4, PMF and DSF	French et al. 2003, 2005, 2007; Demitroff 2016

(Continued)



Review in Advance first posted on  
 March 14, 2022. (Changes may  
 still occur before final publication.)

**Table 3 (Continued)**

General location(s)	Location(s) or town(s) (Universal Transverse Mercator coordinates)	Feature(s) (evidence)	Feature age (technique)	Feature dimensions	Host material (age, lithology)	Paleoenvironmental implication(s)	Citation(s)
Central Pennsylvania, Ridge and Valley, Appalachians	Benfer area quarry (4515522.90 m N, 311018.72 m E)	Ice-wedge pseudomorphs, relict sand wedges, or composite-wedge pseudomorphs (quarry)	Possibly late Pleistocene (inferred from stratigraphy and soil development)	Wedge depths > 1.2 m; widths > 0.5 m (truncated at tops)	Trimmers Rock Formation (Devonian, silstone and shale)	PMF (continuous or discontinuous)	Gardner et al. 1991
Central Pennsylvania, Ridge and Valley, Appalachians	Within ~50 km of State College, Pennsylvania	Ice-wedge pseudomorphs, relict sand wedges, or composite-wedge pseudomorphs (quarry, excavation, or pit)	Unknown	Unknown	Paleozoic limestones and shales	PMF (continuous or discontinuous) and/or DSF	Cronce 1988, Clark & Ciolkosz 1988
Central and southcentral Pennsylvania, Ridge and Valley, Appalachians		Networks of polygonal cracks in shale (air photos, Google Earth imagery, field work)	Unknown	Polygon diameters 5 to ~22 m	Dominantly Martinsburg Formation, also Mauch Chunk Formation (Silurian, Devonian, and Mississippian shales and interbedded shales and silstones)	Possible PMF (continuous or discontinuous)	D. Merritts, J. Marshall, R. Walter, M. Demitroff, N. Hertzler, et al., un- published article
Southeastern Pennsylvania		Networks of polygonal cracks in shale (air photos, Google Earth imagery, field work)	Unknown	Polygon diameters 5 to 13 m; mean diameter $8 \pm 2$ m (n = 31)	Martinsburg Formation (Devonian, shale)	Possible PMF (continuous or discontinuous)	D. Merritts, J. Marshall, R. Walter, M. Demitroff, N. Hertzler, et al., un- published article

(Continued)



Review in Advance first posted on  
March 14, 2022. (Changes may  
still occur before final publication.)

**Table 3 (Continued)**

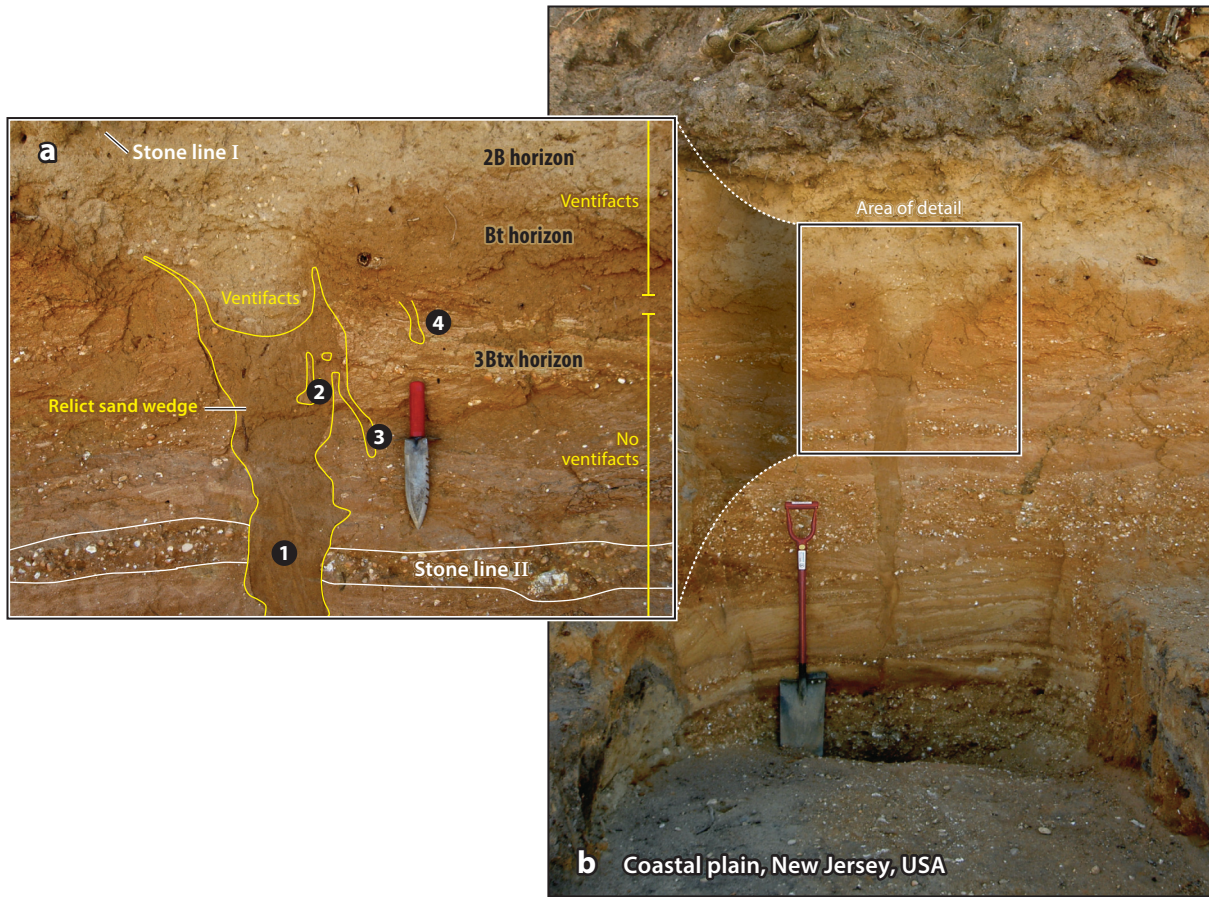
General location(s)	Location(s) or town(s) (Universal Transverse Mercator coordinates)	Feature(s) (evidence)	Feature age (technique)	Feature dimensions	Host material (age, lithology)	Paleoenvironmental implication(s)	Citation(s)
Southeastern Pennsylvania	Schlusser, Pennsylvania, south side Enola Road (Route 944; 4400246.00 m N, 315319.00 m E)	Relict sand wedge or possibly composite-wedge pseudomorph (OSL)	14.9 ± 1.7 ka, interpreted as LGM, possibly also older (OSL, 2 samples, weighted mean age)	Depth ~1.8 to 2 m; diameter up to 30 cm at top of wedge	Martinsburg Formation (Devonian, shale)	PMF (probably continuous)	D. Merritts, J. Marshall, R. Walter, M. Demiroff, N. Hertzler, et al., un- published article; other relict wedges observed but not sampled
New Jersey, Delaware, eastern Maryland (Coastal Plain)		Networks of polygonal cracks in Cenozoic sediments (Google Earth imagery)	Unknown, interpreted as possible LGM	Polygon diameters 10 to >30 m (>160 sites)	Coastal Plain sediments (Cenozoic)	Interpreted as $\leq$ -6°C MAAT	Gao 2014; various wedges are reported here by French et al. 2007, 2009
Central Maryland, Washington, DC, northern Virginia (Coastal Plain– Piedmont)	Millersville, Maryland, Conaway's Reliable Contracting pit, 39°2'N; 76°41'W; near Brandywine, Maryland, Accokeek pit, 38°40'N; 76°55'W; Tysons Corner, Virginia, Havre de Grace, Maryland	Millersville—relict sand wedges; Brandywine— frost cracks; Tysons Corner and Havre de Grace— thermokarst- deformed wedges	Late Pleistocene	Wedge depths 0.5 to 2.0 m; widths 0.1 to 0.3 m (deformed wedges ~2.0 m deep $\times$ ~2.0 m wide)	Coastal Plain sediments (Cenozoic) Piedmont underlain by hard, crystalline igneous and metamorphic rocks	PMF into southern Delaware and central Maryland; discontinuous PMF or DSF south of latitude 38°	Nikiforoff 1955, Conant et al. 1976, French et al. 2009, French 2011
Southern New Jersey, Pine Barrens	Indian Branch, Penny Pot, New Jersey, 39.55435°N, -74.81879°	Networks of polygonal icy cracks in sediments behind 28 ka dune damming (French & Demiroff— 1931 aerials; Demiroff et al. 2019 lidar)	Late Wisconsinan	Polygon diameters 5 to 30 m	Coastal Plain Late Wisconsinan stream terrace deposits	PMF, LGM	French & Demiroff 2012, Demiroff et al. 2019

<sup>a</sup>Murton (2013; personal communication January 10, 2022) refers to ground-wedge casts as seasonal frozen ground ice-vein or composite-vein pseudomorphs.

Abbreviations: DSF, deep seasonal frost; LGM, Last Glacial Maximum; MAAT, mean annual air temperature; MIS, marine oxygen isotope stage; OSL, optically stimulated luminescence; PMF, permafrost.



Review in Advance first posted on  
March 14, 2022. (Changes may  
still occur before final publication.)

**Figure 8**

Relict sand wedge in the Coastal Plain, New Jersey. (a) Upper part of relict sand wedge, with Last Glacial Maximum and greater than marine oxygen isotope stage 4 age from optically stimulated luminescence dating (French et al. 2003, 2005, 2007; Demitroff 2016). Note the minimal downward or upward warping of stone line II and structural features that include (1) sand laminae, (2) host inclusions, (3) sand-vein offshoot or wedge apophysis, and (4) elementary sand vein in fragipan. (b) Full view of the relict sand wedge, with a box indicating the area of panel *a*. Photos courtesy of Mark Demitroff.

(see **Figure 9**). They have orthogonal or hexagonal patterns, and most are 10–30 m in diameter. Gao (2014) compared aerial photos acquired at multiple dates, revealing that polygonal networks are visible only at certain times of the year, probably as a consequence of strong contrasts in soil moisture between fine sediment in wedges and surrounding host material (see **Figure 10**).

Gao's (2014) work extended southward the earlier mapping of Walters (1978), who used aerial photos taken during a drought that revealed traces of thermal contraction polygon networks in Triassic shale in the northern New Jersey Piedmont (see locations in **Figures 1a** and **9**). In addition, Walters (1978) did extensive field work in which he mapped 250 frost wedge features, describing and sketching many from excavations. The wedges have many similarities to sand or composite wedges, although Walters (1978) interpreted them as possible ice-wedge casts (M. Demitroff, personal communication). Walters (1978) had no age control for any of the wedges but inferred that they were late Pleistocene based on their appearance.



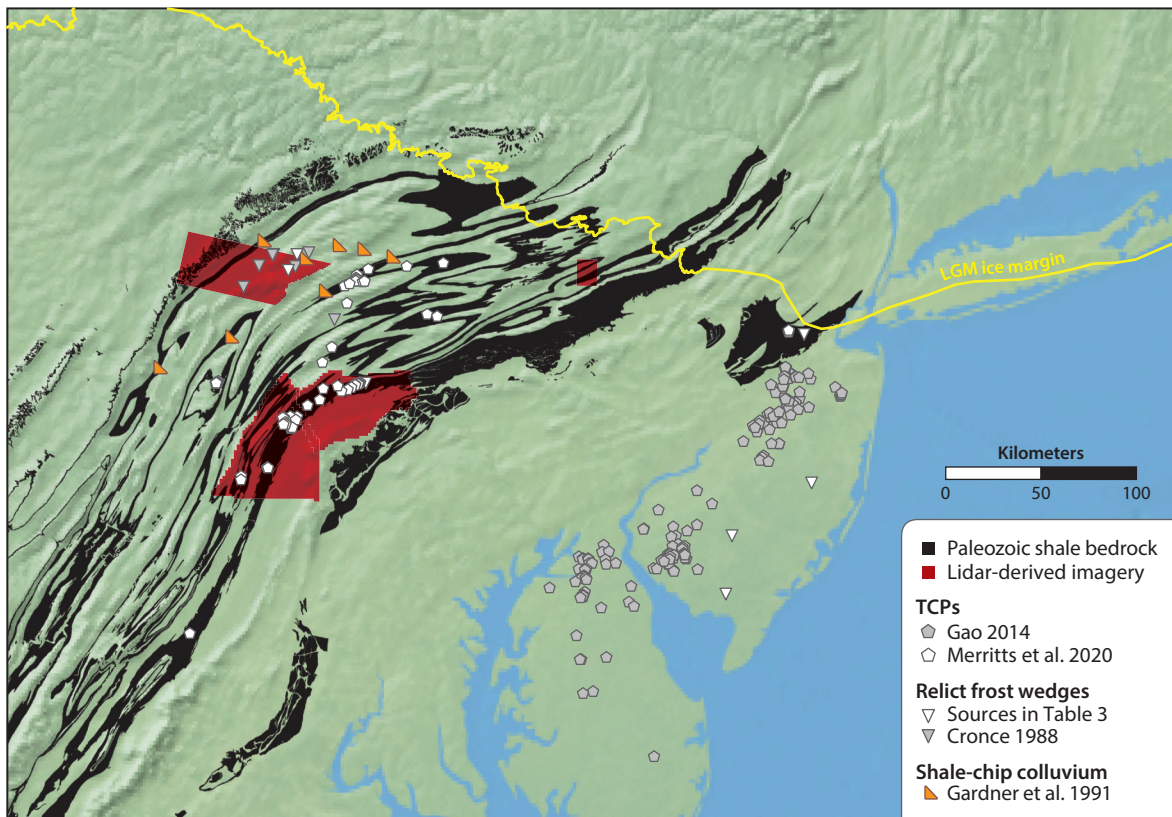


**Figure 9**

Compilation of traces of relict thermal contraction polygons from Gao (2014) and Merritts et al. (2020), relict frost wedges (see Table 3), and shale-chip colluvium sites from Gardner et al. (1991, table 1) for the eastern United States. The red polygons are areas for which we have developed imagery from a 1-m lidar-derived digital elevation model that includes a typical hillshade and a composite terrain rendering of a hillshade, slope map, and map of local flow divergence. The composite terrain rendering highlights slope transitions and high-frequency, low-relief surface textures that can be difficult to visualize otherwise. This imagery is available in online visualizations built on Mapbox (<https://topomatrix.com/mapbox/>; see the **Supplemental Video**), where the viewer can switch from standard hillshade to composite terrain views and toggle on and off USDA soil data and surficial geologic mapping units (see the sidebar titled Mapbox Note). Sites of relict periglacial features (thermal contraction polygons and frost wedges) also are located in the Mapbox imagery.

In the Appalachian region (mostly the Valley and Ridge), Merritts et al. (2015, 2020) and D. Merritts, J. Marshall, R. Walter, M. Demitroff, N. Hertzler, et al. (unpublished article) followed Gao's (2014) approach, using multiple years and seasons of Google Earth and other aerial imagery to map traces of thermal contraction polygon networks at more than 50 sites, all in shale bedrock or its colluvium (Figures 7c and 11a,b). Some are in New Jersey (near the sites of Walters 1978) and Maryland, but most were mapped throughout central Pennsylvania. The majority of these thermal contraction polygon networks are orthogonal, with diameters of ~6–30 m. Merritts et al. (2015) began by searching areas with earlier reports of frost wedges from central Pennsylvania (particularly that of Gardner et al. 1991). These sites yielded numerous traces of thermal contraction polygon networks, especially with September imagery (see Figure 7c). From there, Merritts et al. (2020) and D. Merritts, J. Marshall,



### MAPBOX NOTE

As part of this review, we provide imagery at Mapbox (<https://topomatrix.com/mapbox/>; see the **Supplemental Video**) for the reader to explore periglacial landscape legacies at the three areas shown in red in **Figure 9**. Calculated from a 1-m lidar-derived digital elevation model, the imagery includes a typical hillshade as well as one that is a composite of a hillshade, slope map, and map of local flow divergence. The composite terrain rendering highlights slope transitions and high-frequency, low-relief surface textures that can be difficult to visualize otherwise. The viewer can switch from standard hillshade to composite terrain views and add layers that include USDA colluvial and residual soils data for central Pennsylvania and mapped surficial deposits for an area near the Last Glacial Maximum ice margin (mapping from Braun 1996). Also included are all thermal contraction polygons from Merritts et al. (2020); Gao (2014); and D. Merritts, J. Marshall, R. Walter, M. Demitroff, N. Hertzler, et al. (unpublished article) and frost wedges from Cronce (1988); Merritts et al. (2020); and D. Merritts, J. Marshall, R. Walter, M. Demitroff, N. Hertzler, et al. (unpublished article). The viewer can see firsthand the range of legacies of periglacial features, including distinct solifluction lobes and terraces and possible detachment slides and retrogressive thaw slumps.

R. Walter, M. Demitroff, N. Hertzler, et al. (unpublished article) mapped thermal contraction polygon in shale terrain into northern Maryland, where they become difficult to locate. The swath of thermal contraction polygon networks is similar in extent (~200–250 km from north to south) to that of Gao (2014) for thermal contraction polygon networks mapped to the east in the MACP and overlaps the mapping of speculative LGM permafrost of French & Millar (2014) (compare **Figures 1a** and **9**).

Fissile, highly fractured Paleozoic shales contain the most distinctive and numerous traces of thermal contraction polygons (Merritts et al. 2020; D. Merritts, J. Marshall, R. Walter, M. Demitroff, N. Hertzler, et al., unpublished article) (see **Figures 7c**, **9**, and **11**). Many of the orthogonal thermal contraction polygon borders closely follow two preexisting bedrock fractures sets for folded rocks in the Appalachian region (~60–70° and 140°). The majority of polygon networks occur on the tops of shale benches or at upper- to mid-slope locations. It is likely that more exist downslope but have been buried by colluvium, perhaps during the period of late LGM permafrost thaw, as confirmed by descriptions of buried frost wedges in a shale quarry in central Pennsylvania (Gardner et al. 1991).

**Coastal plain, New Jersey, USA**



**Figure 10**

Thermal contraction crack polygon trace remains in Coastal Plain sediments near Sharon, northern New Jersey (40 km south of Last Glacial Maximum ice margin) (site 160 of Gao 2014). (a) Google Earth image from September 6, 2013. Polygon traces cannot be detected. (b) Random orthogonal polygons can be detected from September 20, 2010, imagery. (c) Line drawing of photo in panel b. Panels b and c adapted with permission from Gao (2014), figure 2b.



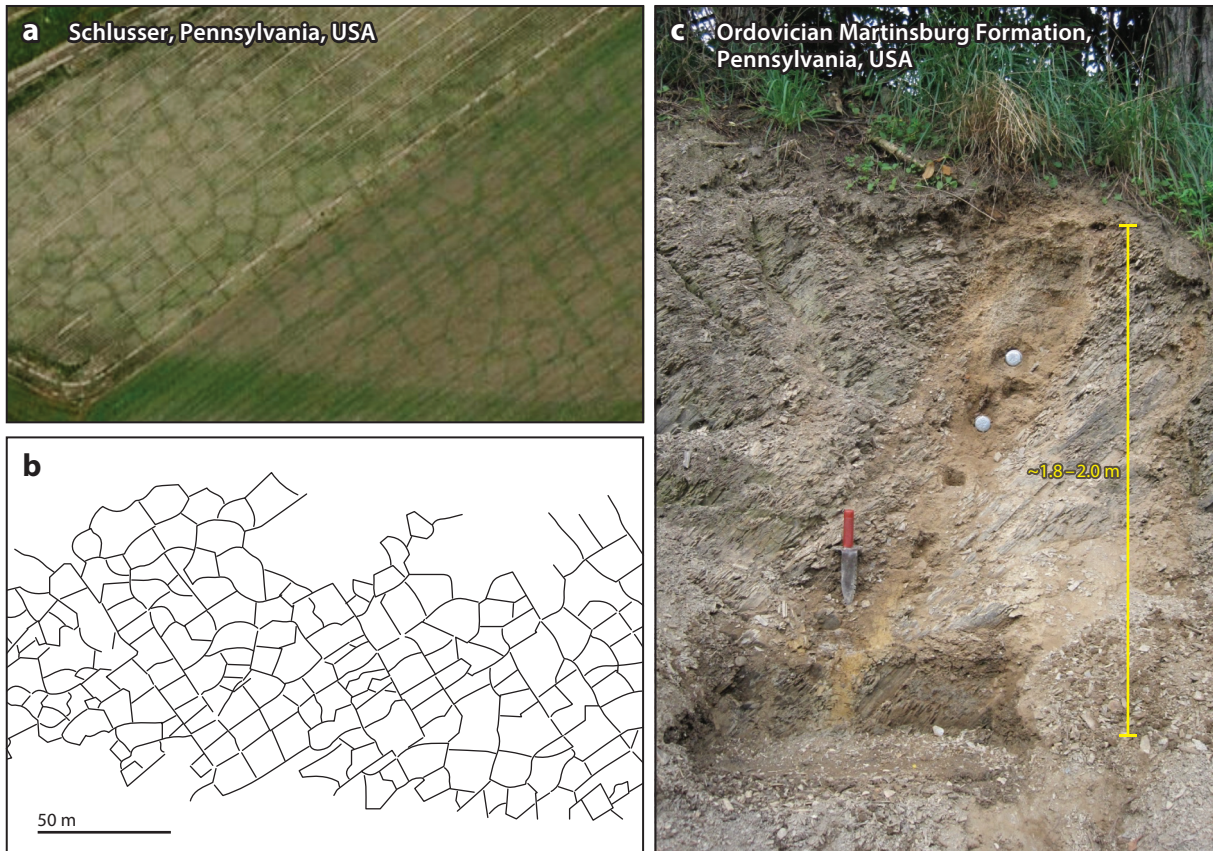


**Figure 11**

(a) Trace remains and (b) line drawing of thermal contraction crack polygons with relict sand wedges in central Pennsylvania, near the site of Gardner et al. (1991) ~70 km south of the Last Glacial Maximum ice margin. The polygons occur in Devonian Trimmers Rock Formation shale. (c) Relict sand wedge exposed in a road cut near Schlusser, Pennsylvania (4460246.00 m N, 315319.00 m E). The wedge formed along a fracture in highly brecciated Ordovician Martinsburg Formation shale. The depth of the wedge is ~1.8 to 2 m; the diameter is up to 30 cm at the top of the wedge. Optically stimulated luminescence ages of the sandy infill are  $14.9 \pm 1.7$  ka (S. Huot, unpublished data), interpreted as Last Permafrost Maximum in age (D. Merritts, J. Marshall, R. Walter, M. Demitroff, N. Hertzler, et al., unpublished article).

### Ice-Wedge Pseudomorphs and Relict Sand Wedges in the Appalachian Region

Several field-based studies of thermal contraction polygons and relict sand wedges in central and eastern Pennsylvania, within the area mapped for thermal contraction polygons in shale by Merritts et al. (2020) and D. Merritts, J. Marshall, R. Walter, M. Demitroff, N. Hertzler, et al. (unpublished article), were completed after the work of Péwé (1983) and included in the French & Millar (2014) analysis (see **Table 3**). A detailed sedimentologic and geomorphologic study at a quarry in central Pennsylvania, ~70 km south of the LGM ice margin, described frost wedges with truncated tops and an erosional unconformity in greater than 10 m of toe-of-slope stratified shale-chip colluvium (Gardner et al. 1991) (**Figure 12**). The wedges have similarities to composite wedges and are buried by up to several meters of younger, slope-stratified shale-chip colluvium in which sediment is undeformed (i.e., no cryoturbations) and has no relict wedges (Gardner et al.



**Figure 12**

Shale quarry near Benfer, central Pennsylvania (4515522.90 m N, 311018.72 m E), with slope-stratified shale-chip colluvium and relict frost wedges (from Gardner et al. 1991). See **Table 3**. (a) View of quarry looking west, showing typical mid-Atlantic region Ridge and Valley physiographic province landscape, with sandstone (orthoquartzite) ridges in the distance and low rounded shale benches in the foreground (Devonian Trimmers Rock Formation). Photo courtesy of Thomas Gardner. (b) Photograph of the eastern wall of the upper bench in the shale quarry, showing erosional unconformity between two colluvial units (*top of hammer*). The relict frost wedge formed in the lower unit is truncated. Its light color is due to vertically reoriented framework grains along the frost crack face and well-developed silt loam coatings on clasts. Photo reproduced from Gardner et al. (1991).

1991) (see **Figure 12b** and **c**). The source of the colluvium is immediately upslope (<300 m), from a low-relief (~20 m) shale hill with short, gentle (~4°) slopes, presumably from frost-shattered rock. Below we discuss brecciated shale nearby that is associated with deep periglacial frost cracking (West et al. 2019).

Relict frost wedges in shale and limestone were described at more than a dozen sites within tens of kilometers of this site in central Pennsylvania (Cronce 1988) (see **Figure 9** and **Table 3**), and Marsh (1999) described hexagonal and orthogonal thermal contraction polygon networks (10-m-diameter polygons) on low benches of Devonian shale with truncated sand wedges—some at least 1.5 m deep—in eastern Pennsylvania. No age control was obtained for periglacial features at any of these sites.

A sand wedge at a road cut (Route 944) along a low-relief (<3 m) shale bench just south of Blue Mountain in southeastern Pennsylvania provides the first known age control for a sand wedge in the Appalachian region (Gross 2017; D. Merritts, J. Marshall, R. Walter, M. Demitroff, N. Hertzler, et al., unpublished article) (**Figure 11c**; location in **Figure 9**). The wedge formed within highly shattered (brecciated) Ordovician Martinsburg shale and follows a preexisting near-vertical fracture trace that trends ~70°. The uppermost part of the wedge appears to be truncated slightly (perhaps from late Pleistocene permafrost thaw) and is overlain by ~0.5 m of shale-chip colluvium. OSL dating of the sandy infill of the greater than 2.0-m-deep sand wedge by Sébastien Huot yielded a LPM age estimate of  $14.9 \pm 1.8$  ka [1-sigma weighted mean age for two OSL dates at depths of 0.9 m and 1.2 m below ground surface (D. Merritts, J. Marshall, R. Walter, M. Demitroff, N. Hertzler, et al., unpublished article)].

## EVIDENCE OF INTENSE FROST ACTION AND REPEATED FREEZING AND THAWING

We now turn our attention to landforms and deposits that indicate former conditions of intense frost action and repeated ground freezing and thawing (see **Tables 1** and **2**). A general conceptual model of bedrock fracture and production of regolith that becomes available for downslope transport begins with near-surface ice segregation, rock fracture, and heave in perennially frozen ground during cold periods. Alternating build up and decay of an ice-rich layer leads to fracturing that supplies shattered rock fragments to the active layer during thaw. With continued rock damage, loosened fragments become part of the mobile regolith, available for vertical and lateral sorting into patterned ground, additional weathering, and downslope transport by mass wasting (Murton et al. 2006, Anderson et al. 2013).

Bedded sedimentary rocks in the Appalachian uplands have experienced several episodes of tectonic orogenesis and contain many preexisting rock weaknesses (bedding planes, fractures, and faults) when they reach the critical zone, the zone at Earth's land surface extending from the top of the vegetation canopy through soil to subsurface depths at which fresh groundwater freely circulates. Given that conditions suitable for permafrost existed during late Pleistocene time in the MAR, frost cracking associated with ice segregation is likely to have produced highly brecciated rock and loose regolith that became available for entrainment and mobilization downslope, ultimately the mobile regolith that can become colluvial diamictons (Lebedeva et al. 2010, Riggins et al 2011, Anderson et al. 2013).

### Segregation Ice and Frost Shattering

Ground cooling and freezing can lead to mechanical disintegration and brecciation of coherent rock by formation of segregation ice (Mackay 1999, Murton 1996, Murton et al. 2006, French



2017b) (see **Table 1**). Whereas cracking associated with thermal contraction of frozen substrates generates relatively widely spaced, large vertical cracks and wedges, the growth of millimeter- to centimeter-thick ice lenses of segregation of ice produces small, closely spaced fractures parallel to the ground surface (normal to the direction of freezing) in moist frost-susceptible rock (Murton 1996, Murton et al. 2006, Murton & Ballantyne 2017). Segregation ice can expand and extend preexisting fractures in porous bedrock near the permafrost table, resulting in a highly efficient means of shattering rock (Walder & Hallet 1985, Matsuoka & Murton 2008, Hallet et al. 1991, Murton et al. 2006, Rempel et al. 2016, Draebing & Krautblatter 2019).

Ice segregation cracking occurs in an ice-enriched layer in the uppermost ~10 m or less of freezing or frozen rock and regolith (Walder & Hallet 1985; Hallet et al. 1991; Murton 1996; Murton et al. 2001, 2006). A temperature gradient-induced suction enables unfrozen water to migrate in thin films through partially frozen, porous material toward freezing sites where lenses and layers of ice grow at subzero temperatures. Provided that liquid water is available to migrate to sites of ice growth, frost cracking is a significant process at temperatures from  $-3$  to  $-8^{\circ}\text{C}$ , the frost cracking window (similar to the temperatures for continuous permafrost), although it is not limited to this range (Walder & Hallet 1985, 1986; Hallet et al. 1991; Anderson 1998; Murton et al. 2006; Matsuoka & Murton 2008; Vlahou & Worster 2015; Rempel et al. 2016). Progressive microcracking of rock continues as ice lenses grow, with cracks propagating and intersecting to form brecciated rock, a particularly effective process near the base of the active layer and top of permafrost (Hall et al. 2002). Total rock damage is roughly proportional to the cumulative amount of time that rock spends in the frost cracking window.

Rate of freezing and duration of subfreezing temperatures are significant parameters for frost cracking (Anderson 1998, 2002). Hales & Roering (2007, 2009) proposed that the rates of growth for segregation ice and cracking are proportional to the temperature gradient; hence, the amplitude of seasonal temperature changes is important (Anderson 1998, 2002; Marshall et al. 2015, 2021). This work led to the concept of crack intensity as a proxy for magnitude of frost cracking. Crack intensity is the product of time spent in the frost cracking window and the temperature gradient, calculated for multiple time steps (e.g., one day), integrated over depth, and summed for a full year (units of  $^{\circ}\text{C}/\text{cm}$ , with time implicit). More recently, frost weathering is calculated as depth-integrated annual change in rock porosity (i.e., expansion) (Rempel et al. 2016). Most modeling efforts predict that frost cracking effectiveness peaks at depths of 3 to 10 m below the surface in permafrost conditions (Hales & Roering 2007, Anderson et al. 2013, Rempel et al. 2016).

This approach based on rock porosity was used to generate the map shown for the MAR with LGM climate simulations (Marshall et al. 2021) (**Figure 1b**) and suggests a wider zone of cold-climate frost processes in the MAR than the permafrost limit mapped by French & Millar (2014) (see **Figure 1a**). The zone of intense frost weathering and increased rock porosity modeled by Marshall et al. (2021) is up to three times greater in area. An explanation for the difference is that the frost weathering model reveals a region that has been affected by intense cold-climate conditions and frost action, but has not been sufficiently cold to result in persistent permafrost.

Experiments that simulate natural freezing regimes and frost cracking in wet chalk (Murton et al. 2006) produce bedrock fractures with depths and geometries that match those in modern permafrost environments (Mackay 1999, French 2017b). These experimental and modern cold-region fractures are similar to those in weathering profiles of bedrock in formerly periglacial regions: Numerous mostly horizontal to subhorizontal fractures occur in the upper 0.5 to several meters of bedrock, decreasing in frequency with depth (Murton 1996, Murton et al. 2006).



## Investigations of Bedrock Fracturing from Ice Segregation at the Susquehanna Shale Hills Critical Zone Observatory, Pennsylvania

A detailed study of shale weathering at the Susquehanna Shale Hills Critical Zone Observatory (SSHCZO) (Brantley et al. 2018) (see **Figure 9**) identified a zone of fine fractures that diminish in frequency and increase in spacing in the uppermost ~6–7 m of bedrock (West et al. 2019). Intense weathering was attributed to segregation ice growth and frost cracking during periglacial conditions and supports the notion of former existence of permafrost (West et al. 2019). The site is located in Silurian shale about 75 km south of the LGM ice margin, near multiple relict frost wedges (Cronce 1988, Gardner et al. 1991) and thermal contraction polygons (Merritts et al. 2015, 2020; D. Merritts, J. Marshall, R. Walter, M. Demitroff, N. Hertzler, et al., unpublished article).

Research at the SSHCZO provides an exceptionally rich record of long-term rates of regolith production and erosion (Jin et al. 2010; West et al. 2011, 2013, 2014) and periglacial weathering (West et al. 2019). Multiple techniques used to characterize the watershed's subsurface architecture included direct borehole observations with optical televiewer logs, shallow seismic refraction and ground penetrating radar surveys, and geochemical attributes of subsurface samples (Kuntz et al. 2011, Guo et al. 2014, Slim et al. 2015, Sullivan et al. 2016, Gu et al. 2020, Ma et al. 2021). Zones of intense fracturing were observed in all wells, with peak fracture densities from ~2 to 5 m below the land surface. The lower boundary (~7–8 m) marks a transition zone between fractured, weathered regolith and relatively unweathered bedrock with few fractures (West et al. 2019).

Models of frost cracking based on paleoclimate data (MAATs between 0 and –10°C with temperature swing amplitudes of 10–20°C) reveal that frost cracking could have occurred to depths greater than 10 m (West et al. 2019). Most model runs, however, generated peak frost cracking potential at depths of 5 to 8 m below the land surface and aligned with observed peak fractures. Comparing their model results with data from hillslope P-wave tomography and modern permafrost environments, West et al. (2019) found that south-facing slopes in the watershed correlate most closely with paleotemperature estimates of –2.5°C MAAT, and north-facing slopes with estimates of –5 to –7.5°C. These differences in aspect-related insolation explain the observed topographic asymmetry in the watershed, in which cooler north-facing slopes are steeper than warmer south-facing slopes by about 5° and generally have thicker regolith (Ma et al. 2010, 2013; West et al. 2013, 2014).

## Mobile Regolith: Spatial Extent of Colluvial Diamictons and Early Work Invoking Solifluction

During oscillating periods of Quaternary warming, ice-rich fractured layers that formed during cold periods would have completely thawed, leading to thaw settlement of the ground surface and enhanced mobile regolith transport via multiple mass wasting processes (Murton et al. 2006, Anderson et al. 2013). With each time step of regolith stripping, deeper bedrock is exposed in the weathering profile to experience the next round of frost shattering, resulting in the repeated layers of colluvium consisting of clasts of sandstone and shale so commonly reported in the MAR (e.g., Gardner et al. 1991, Braun et al. 1994, Pazzaglia & Cleaves 1998) (see **Figure 12**).

Approximately 70 km east of the SSHCZO, for example, the ~20-m-thick toe-of-slope stratified shale colluvium with frost wedges described by Gardner et al. (1991) documents repeated regolith stripping, as well as a record of damage done by frost cracking in bedrock a short distance (<300 m) upslope. The highly fissile shale bedrock was frost susceptible, leading to intense brecciation of rock and production of readily transported regolith consisting of pebble-sized clasts. Hundreds of thin beds (<20 cm) alternate between silty matrix-supported facies with mean shale chip sizes of 2–5 mm and clast-supported facies with mean clast sizes of 2–13 mm. Based



on multiple sedimentological criteria, Gardner et al. (1991) associated the alternating facies with sheetwash and solifluction, respectively.

Many workers have documented widespread, near-continuous colluvium up to tens of meters thick in the MAR, mapping it mostly as matrix-supported diamictons (Denny 1951, 1956; Braun 1989, 1996; Braun et al. 1994; Pazzaglia & Cleaves 1998; Grote & Kite 2010; Newell & DeJong 2011). Such colluvium extends far south of late Pleistocene glacial limits (Denny 1951, 1956; Becher & Root 1981; Kite 1987; Clark & Ciolkosz 1988; Gardner et al. 1991; Snyder & Bryant 1992; Braun et al. 1994; Grote & Kite 2010; Merritts et al. 2014, 2015, 2020; Del Vecchio et al. 2018; D. Merritts, J. Marshall, R. Walter, M. Demitroff, N. Hertzler, et al., unpublished article). Early mapping of these features lumped them with solifluction, as in Péwé's (1983) compilation of solifluction deposits and other colluvia (see **Figure 1a**).

The extent (e.g., percent of ground cover or distance from source rock) and thickness of colluvium generally decrease southward, away from Pleistocene ice sheet margins. Near ice sheet margins in northern Pennsylvania, for example, Braun (1996) documented boulder colluvium greater than 30 m in thickness at toe-of-slope locations derived from upslope sandstone and conglomerate sources (see unit Qbc in **Figure 13**). In the same region, on slopes as gentle as 1°, Braun et al. (1994, p. 36) observed that nearly all parts of the landscape are mantled in a sheet that covers essentially all slopes more or less evenly in colluvium, suggesting a process that “fluidizes the material” and is interpreted by the authors to be periglacial gelification. Braun et al.'s (1994) description resembles one for active solifluction from Signy Island, Antarctica, where Holdgate et al. (1967, p. 60) reported solifluction “on such a vast scale that it is often difficult to realize that it is happening. Whole slopes are in motion....”

In central Pennsylvania, Ciolkosz et al. (1986a,b) documented that all but the uppermost parts of slopes in the MARVAR are mantled with colluvium that varies from 0.5 m to more than 30 m in thickness, extending downslope on average about 1 km from ridge crest sandstone source rocks (**Figure 14**). The material on the upper quarter of slopes typically is mapped by geologists and soil scientists as rubble, probably akin to modern understanding of freshly produced mobile regolith (e.g., Anderson et al. 2013). Ciolkosz et al. (1986a,b) estimated that 27% of soils in unglaciated central Pennsylvania are formed in periglacial colluvium. Given the stratigraphy of folded sandstone, shale, and limestone in the MARVAR, the cobble to boulder sandstone colluvium generally overlies shale at mid-slope to toe-of-slope locations, and sometimes even limestone along lower valley margins (see **Figure 14**).

Several early workers invoked solifluction in describing these colluvial diamictons (Denny 1951, 1956; Potter & Moss 1968; Moss 1976; Braun et al. 1994). In central Pennsylvania Carter & Ciolkosz (1986, p. 245) described a slope as covered in meter-scale lobate terraces (5–30 m long and similar in width) that they viewed as “identical in form” to active solifluction lobes in the Arctic region. At this site, depth to bedrock determined from 16 hammer seismograph lines and 19 soil pits ranged from 3.0 to 6.3 m and was interpreted to be the result of deep frost weathering. It is probably not a coincidence that many reports of depth to bedrock in the region are within this range (e.g., West et al. 2019) and are similar to descriptions of depths of brecciated rock produced from ice segregation by Murton (1996) and Murton et al. (2006).

Farther south in Maryland, West Virginia, and Virginia, cobble to boulder matrix-supported diamictons have been mapped as aprons along lower slopes as well as in debris and alluvial fans (Kite 1987, Eaton et al. 2003a, Smoot 2004, Taylor & Kite 2006, Grote & Kite 2010, Chilton & Spotila 2020). In general, Pleistocene and Holocene debris flows are more common than to the north (Kochel & Johnson 1984; Eaton et al. 2003a,b). Furthermore, solifluction landforms (sheets and lobes) are less pronounced than to the north in Pennsylvania (Merritts et al. 2015, 2020; D. Merritts, J. Marshall, R. Walter, M. Demitroff, N. Hertzler, et al., unpublished article). In Virginia,





(Caption appears on following page)



**Figure 13** (*Figure appears on preceding page*)

(a) Composite of a hillshade, slope map, and map of local flow divergence near Nesquehoning, Pennsylvania, ~13 km from the Last Glacial Maximum ice margin, available at MapBox (<https://topomatrix.com/mapbox/>). The composite terrain rendering highlights slope transitions and high-frequency, low-relief surface textures that can be difficult to visualize otherwise (e.g., with conventional digital elevation model hillshade). The box shows the area of panel b. (b) Map units of surficial geologic deposits from Braun (1996). Qbm is Quaternary boulder mantle overlying a clast-supported diamict. Boulders are up to 2 m long, and cobbles cover more than 75% of ground surface. Deposit is usually less than 1 m to bedrock. Qbc is Quaternary boulder colluvium overlying mostly matrix-supported diamict. Boulders are up to 5 m long, and cobbles cover 25–75% of ground surface. Deposit is usually 2–10 m thick and may exceed 30 m. Qcm is Quaternary cobble mantle overlying clast-supported diamict or sometimes matrix-supported diamict. Cobbles and occasional boulders cover more than 75% of ground surface. Usually it is less than 1 m to bedrock. Qssc is Quaternary stony colluvium derived from gray sandstone, matrix-supported diamict, and slope-parallel (long axis) clasts and lenses. Clasts are 0.1–0.25 m long and cover more than 25% of ground surface. Deposit is usually 2–5 m thick. Colluvium fills small valleys and headwater areas of tributaries and occurs as coalescent lobes at toe-of-slopes. Qsrc is the same as Qssc but for red sandstone. R is clast-rich diamict of residual and colluvial material derived directly from underlying bedrock of sandstone and shale. Clasts are typically matrix-supported, with strong slope-parallel orientation. The depth to bedrock is less than 1–2 m. The inset photo in the lower left is of solifluction terraces in Alaska. (c) Topographic profile A–A', with location shown in panel b, showing four solifluction terraces with risers ~4–8 m in height, spaced ~150–300 m apart.

Chilton & Spotila (2020) mapped sandstone boulder distributions associated with periglacial deposits in the MARVAR using unmanned aerial vehicle (drone) imagery and field observations. Large (>1 m average, up to 6-m diameter) boulders sourced from sandstone ridge crests cover up to 9% of hillslopes but are as highly concentrated as 90% in valley bottoms, armoring both and stabilizing topography over multiple Pleistocene climate cycles. For hillslopes, however, the spatial coverage of boulder colluvium is much less than that of central and northern Pennsylvania.

### Age Control for Pleistocene Colluvial Diamictons

Age control for late Pleistocene colluvium in the MAR is scant. Several studies in West Virginia and Virginia, however, link colluvial deposits to Wisconsin cold periods. Radiocarbon dating of organic interbeds within colluvium in West Virginia indicates hollow filling by colluviation during the middle Wisconsin [e.g., >39,320–33,800 years BP (Grote & Kite 2010)]. Nearby sites indicate the onset of colluviation as early as ~31,000 years BP and cessation by ~16,000 years BP [i.e., ~MIS 2 (Behling et al. 1993, Grote & Kite 2010)]. In the Virginia Blue Ridge to the east, Eaton et al. (2003a) bracketed Late Wisconsin depositional ages for ~6.5 m of thinly bedded slope-stratified deposits in a relict debris fan with radiocarbon dates of 24,570–15,800 years BP (i.e., MIS 2), although the upper ~1 m of the deposit was undated and might be younger. Nearby, Eaton et al. (2001) dated organic matter in slope deposits from ~27,410 to 24,450 years BP. In sum, colluvium ages range from about 39,000 to 16,000 years BP and are correlated with MIS 2–3.

Cosmogenic isotopes can be used to constrain exposure ages and the erosional and depositional histories of surficial deposits (see sidebar titled Case Study of the Hickory Run Boulder Field, Pennsylvania, and Similarities to Falkland Island Stone Runs). Along Tussey Mountain in central Pennsylvania, where bedrock is Silurian Tuscarora Formation orthoquartzite, Del Vecchio et al. (2018) modeled postburial nuclide production and decay in quartz in boulder-rich sandy colluvium from an ~9-m core at Garner Run. Del Vecchio et al. (2018) inferred from  $^{10}\text{Be}$  and  $^{26}\text{Al}$  concentrations that at least two pulses of colluvial deposition for the uppermost 6.4 m of sediment might have occurred since  $340 \pm 80$  ka, spanning three glacial cycles, and that the upper 3.9 m of sediment were likely deposited since ~80 ka.

At nearby Bear Meadows, a significant record of late Pleistocene periglacial history associated with cold-climate processes comes from an ~18-m toe-of-slope core, several nearby cores from a bog, and subsurface geophysical investigations (Del Vecchio 2021, Del Vecchio et al. 2021). Concentrations of  $^{10}\text{Be}$  and  $^{26}\text{Al}$  for boulder-rich sediment and underlying saprolite from the



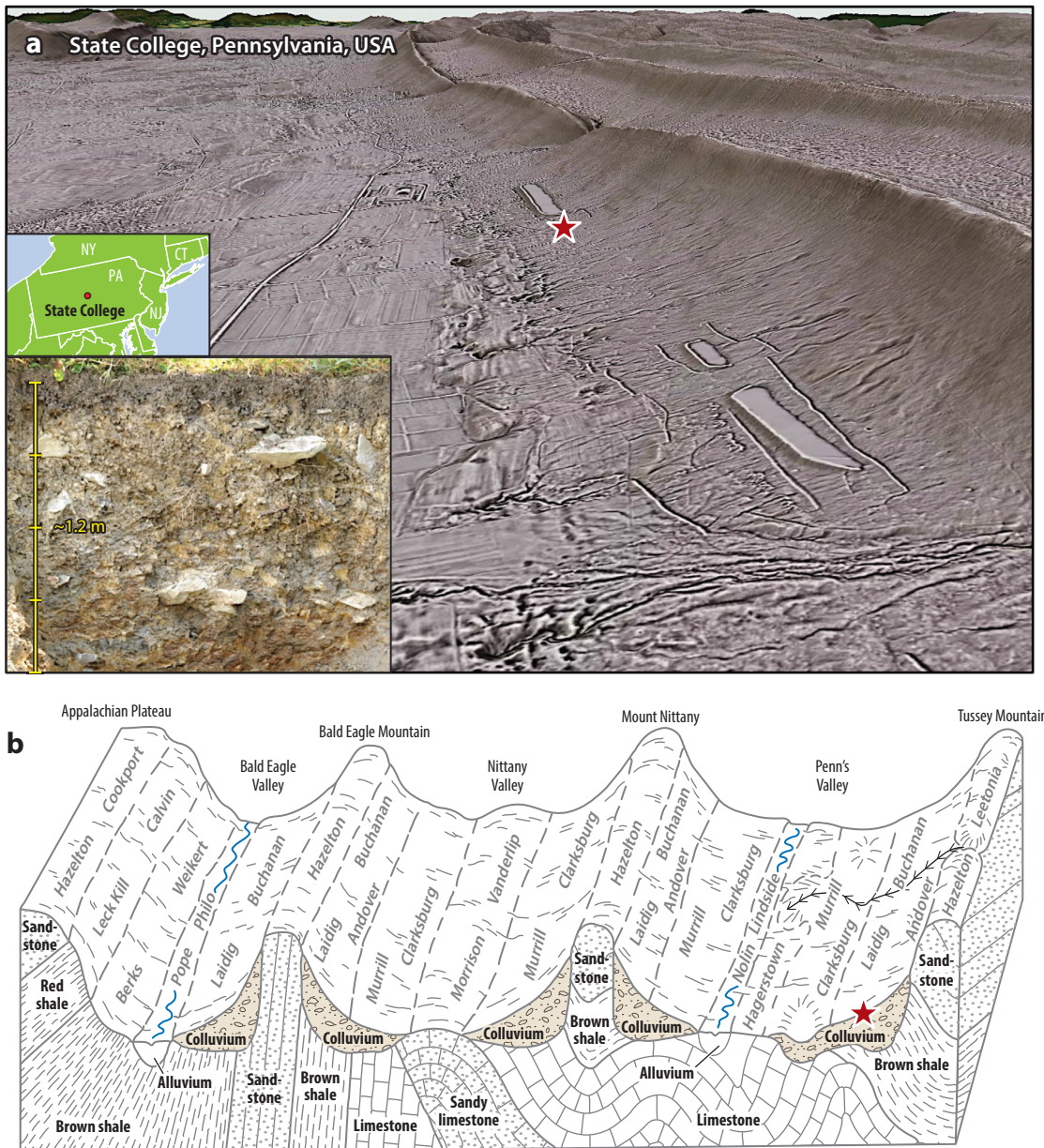


**Figure 14**

(a) Composite of a hillshade, slope map, and map of local flow divergence near State College, central Pennsylvania, ~90 km from the Last Glacial Maximum ice margin, available at MapBox (<https://topomatrix.com/mapbox/>). The view is to the northwest of Tussey Mountain, showing a long colluvium-mantled slope. The inset photo of colluvium from a site near the red star shows USDA Andover series soil formed in sandstone colluvium. The scale bar is 1.2 m high, with 0.3-m spacings. Inset gigapan photo courtesy of Kenneth Tamminga. (b) Schematic of mid-Atlantic region Ridge and Valley physiographic province in State College, central Pennsylvania, showing bedrock units and overlying periglacial colluvium. The red star shows the approximate location of the red star in panel *a* and the inset photo. Figure adapted from Ciolkosz et al. (1986a).



18-m core indicate that erosion rates increased after the onset of 100-ky glacial cycles at the Mid-Pleistocene Transition (1.2–0.7 Ma). As at Garner Run, the upper 3 m of sediment from this core are interpreted to have been deposited since ~80 ka. Based on pollen, geochemical data, radiocarbon dating, and other analyses of cores from the bog, depositional changes in the sedimentary record can be linked to local vegetation and global climate change for the past ~15 ky. These changes indicate that solifluction likely occurred during the Bølling–Allerød warm period (14,690–12,890 years BP), followed by slopewash of fine sediment from adjacent hillslopes during the early Holocene. Fine sediment deposited in the bog before 15 cal ky BP and 13–11 cal ky BP appears to be aeolian, consistent with independent evidence of aeolian enrichment of surficial deposits in the region during periglacial conditions (Lindeburg & Drohan 2019, Drohan et al. 2020).

The Pennsylvania examples using cosmogenic isotopes to constrain exposure and burial histories for Hickory Run (see sidebar titled Case Study of the Hickory Run Boulder Field, Pennsylvania, and Similarities to Falkland Island Stone Runs), Garner Run, and Bear Meadows do not link boulder colluvium conclusively to former occurrence of permafrost, but they do indicate significant frost action and cold-climate processes that are inactive today. Paired with detailed geomorphic mapping and other analyses (Denn et al. 2017, Del Vecchio et al. 2018), these studies document long residence times of regolith with complex exposure and burial histories on hillslopes and valley bottoms, and limited postdepositional erosion.

A study along an ~2-km-long road built in 2019 from the bottom to top of Chestnut Ridge less than 20 km south of the LGM ice margin near Palmerston, Pennsylvania, yielded cosmogenic isotope data from the newly exposed stratigraphy of slope-parallel, meter-scale beds of boulder-rich diamicton in an ~8-m-thick solifluction lobe (Hertzler 2020; Merritts et al. 2020; Ruck 2020; Ruck et al. 2020; D. Merritts, J. Marshall, R. Walter, M. Demitroff, N. Hertzler, et al., unpublished article) (see **Figures 2 and 15**). The lobe is located ~20 m downslope of its source rock (interbedded Devonian sandstone and siltstone), also exposed in the road cut. Concentrations and ratios of in situ  $^{10}\text{Be}$  and  $^{26}\text{Al}$  from the sandy matrix and cobble-sized clasts are consistent with near-surface exposure and burial during only the last glacial cycle and relatively rapid erosion and deposition of colluvium. Stratigraphic features suggest downslope motion by plug-like flow (discussed below) and hence former existence of permafrost.

## PERIGLACIAL MASS MOVEMENT OF MOBILE REGOLITH

Solifluction, a form of slow mass movement, is the most widespread slope-deforming process in modern cold regions and often is associated with lobate landforms (Kinnard & Lewkowicz 2005, Ridefelt et al. 2009) (see **Figures 2 and 3**). We consider the character and distribution of large relict solifluction features in the MAR as a possible indicator of former permafrost or deep seasonal freezing and subsequent thaw. Recall that solifluction and other colluvial deposits were included in Péwé's (1983) mapping of periglacial features for the eastern United States, but only in two places: near the LGM ice margin and much farther south in the Carolinas, with a large spatial gap between (see **Figure 1a**). Furthermore, although French & Millar (2014) viewed solifluction and associated phenomena such as frost-shattered bedrock and colluvium to be clear evidence of frost action, they did not consider them to be conclusive evidence of permafrost, a widely held view. Here, we revisit this view, by examining modern solifluction processes and landforms first, and then relict solifluction features and their spatial extent in the MAR.

### Modern Solifluction Processes and Conditions

Volumetrically, sediment transport on regolith-mantled slopes in periglacial regions is dominated by solifluction associated with recurrent freezing and thawing (Harris 2013, Murton & Ballantyne





**Figure 15** (Figure appears on preceding page)

(*a*) Drone image of Chestnut Ridge, Pennsylvania, with a new road excavated in 2019, ~15 km south of the Last Glacial Maximum (LGM) ice margin. The area is the same as that in **Figure 2**. (*b*) Internal stratigraphy of solifluction bench from the site in the box shown in panel *a*. The bench is less than 20 m downslope of the source bedrock (sandstone and some shale). Markings on the scale bar are 1 m; the total height of the outcrop is ~8 m. Cosmogenic isotope analysis indicates the entire outcrop could have been deposited during the LGM (Merritts et al. 2020; D. Merritts, J. Marshall, R. Walter, M. Demitroff, N. Hertzler, et al., unpublished article). Note the person for scale at the bottom center. (*c*) Depth-velocity profiles for different thermal regimes. Figure adapted from Ballantyne (2018).

2017). Periodically frozen soil is a mixture of granular material, fluid, and ice, hence a complex rheology. Insights on solifluction from global field studies and laboratory experiments show that it occurs in areas with deep seasonal freezing and permafrost, although with different types and rates of movement (Matsuoka 2001, Harris et al. 2008, Harris 2013).

Solifluction consists of several mass movement processes (Harris et al. 1997, 2008; Matsuoka 2001; French 2017b; Ballantyne 2018): frost creep (ratchet-like downslope movement due to segregation ice growth and heave), gelifluction (flow of partially saturated soil during thaw), and plug-like deformation (soil deforming along a slip plane in an ice-rich zone near the base of the active layer). Frost creep occurs in nonpermafrost and permafrost environments, whereas gelifluction is more common where permafrost exists and downward drainage of water from the active layer is limited by frozen ground. Plug-like deformation occurs only in areas of permafrost. Rates of near-surface solifluction movement typically range from 0.5 to 5.0 cm/year but can be as high as ~27 cm/year on steep slopes in areas of high-frequency diurnal frost heave (see compilation of multiple studies in French 2017b). Key variables that control solifluction occurrence, distribution, and transport rates are MAAT, snow depth, vegetation cover, and slope angle (Hjort 2014).

Gelifluction occurs in association with rapid increases in porewater pressure and thaw consolidation of ice-rich ground (Harris et al. 1997, 2001, 2003). Wet, thawed soil has low shear strength and is readily deformed, with strain greatest at the depths of most abundant segregated ice. Concentration of segregated ice depends upon the ground freezing regime (French 2017b). For deep seasonal frost, freezing is one-sided (downward from the surface) during cooling, and segregated ice becomes concentrated near the surface. For areas of cold permafrost, freezing is two-sided, occurring both downward from the surface and upward from permafrost, resulting in ice-rich layers both near the ground surface and at the base of the active layer.

Depth-velocity (strain) profiles of solifluction vary for these different thermal regimes and processes, but most show an exponential decrease in velocity with depth (Matsuoka 2001) (**Figure 15c**). For one-sided freezing, strain declines with depth. For two-sided freezing, the active layer can move en masse (plug-like) if thaw of ice lenses at its base generates sufficiently high porewater pressures (Mackay 1981, Matsuoka 2001, Harris et al. 2011). Strain generally occurs at greater depths and throughout more of the profile where permafrost exists. Physical modeling indicates that volumetric transport rates are two to three times higher in areas of permafrost with two-sided freezing (Harris et al. 2008).

### Solifluction Lobes, Terraces, and Fingering Patterns

Periodically frozen soils moving downslope by solifluction can form uniform sheets but often develop evenly spaced lobes and terraces with thickened fronts (risers) up to about 6 m in height. Downslope wavelengths of lobes and terraces are commonly tens to hundreds of meters, sometimes longer. Pronounced lobate forms occur, for example, in tundra environments where permafrost and two-sided freezing of the active layer are observed (French 2017b). In some cases, however, no surface expression of solifluction exists (e.g., Ridefelt et al. 2009). This is a particularly important observation for those studying relict periglacial deposits (colluvium or regolith)



and solifluction landforms, and is probably why Péwé (1983) lumped the two together in his compilation (see **Figure 1a**). Field studies indicate that some lobes and terraces are turf banked, with vegetated fronts that impede downslope soil movement (Benedict 1976). Others are stone banked, with cobbles and boulders concentrated near lobe fronts and margins. Stone-banked lobes are generally higher than turf-banked lobes, and boulder jamming might be a mechanism for stalled flow and greater heights of sediment.

Some solifluction landforms resemble large-scale fingering patterns that result from instabilities at fluid fronts [e.g., icing dripping from a cake (Glade et al. 2021)]. Such patterns are widely observed in the MAR and discussed in the next section (see **Figures 2a** and 13). These patterns reflect competition between viscous and cohesive forces in periodically frozen soil with high effective viscosity that increases with depth (Glade et al. 2021). Causes of the instabilities might be heterogeneities in topography or material properties on rough substrates. As cohesive lobe and terrace fronts stall on slopes, sediment can accumulate upslope and move laterally toward the sides, building up substantial amounts of mobile regolith. Where permafrost exists, it aggrades upward in response to sedimentation, enabling continued downslope transport associated with active layer thaw near the top of the lobe and hence overrunning older deposits within the underlying sediment (Verpaelst et al. 2017).

Glade et al. (2021) analyzed the morphology of ~3,000 lobes across Norway with lidar-derived digital elevation models (DEMs) and found that lobe thickness and cross-slope wavelength vary with elevation. This finding suggests climate control that is consistent with conditions required for segregation ice growth and frost heave. In essence, certain solifluction features might be highly co-located with frost cracking and brecciated rocks, as the conditions for their formation are similar. Based on 20 years of recent climate metrics, Glade et al. (2021) determined that greater annual air temperature amplitudes and lower MAATs are associated with an increase in lobe thickness and finger wavelength (downslope lobe spacing). These results are interpreted as an indication that climate primarily affects depth of solifluction deposits, which in turn affects lobe wavelengths, and provide a useful analog for interpreting the paleoenvironmental implications of relict solifluction lobes.

### Relict Solifluction Features

Solifluction landforms are a topographic signature of freezing, thawing, and mass movement, just as thermal contraction polygons and frost wedges are of thermal contraction cracking and as brecciated rock is of segregated ice and frost cracking. Solifluction landforms, largely absent in Péwé's (1983) compilation for the eastern United States, were far more abundant than known at the time (Merritts et al. 2013, 2014, 2020; D. Merritts, J. Marshall, R. Walter, M. Demitroff, N. Hertzler, et al., unpublished article). Most lobes in the MAR appear to be of the stone-banked type described in the Rocky Mountains by Benedict (1976). Relict lobes in the MAR are common on the upper thirds to halves of slopes, whereas terraces are common on lower slopes and extend to adjacent valley bottoms, similar to modern solifluction landscapes (e.g., Hauber et al. 2011). Lobes range in height from 1 to 9 m, but terraces along lower slopes are sometimes greater than 15 m in height, probably reflecting sediment added from slopewash and other processes.

Analysis of high-resolution topographic data along the length of Blue Mountain in the MAR reveals that relict solifluction landforms are ubiquitous over a distance of hundreds of kilometers south of the LGM ice margin (Merritts et al. 2014, 2015, 2020; Alter 2015; Hertzler 2020; Ruck et al. 2020; D. Merritts, J. Marshall, R. Walter, M. Demitroff, N. Hertzler, et al., unpublished article). Solifluction landforms diminish in frequency to the south (Merritts et al. 2015, Hertzler 2020), disappearing except at high elevations at the latitude of northern Virginia. In general, the



region of prominent solifluction lobes and terraces is co-located with that of recently mapped thermal contraction polygons (Merritts et al. 2015, 2020; Hertzler 2020; Ruck et al. 2020; D. Merritts, J. Marshall, R. Walter, M. Demitroff, N. Hertzler, et al., unpublished article), the LGM permafrost limit of French & Millar (2014), mapping of boulder-rich colluvial diamictons cited throughout this review, and the spatial distribution of blockfields investigated by Nelson et al. (2007).

In a recent study of hillslope length from lidar-derived 3-m DEMs for anticlinal ridges underlain by Silurian Tuscarora orthoquartzite in Pennsylvania and West Virginia, Del Vecchio (2021) identified a correlation with a modeled paleotemperature gradient based on paleoclimate simulations from the Community Climate System Model version 3 (CCSM3) (Lorenz et al. 2016). Del Vecchio (2021) determined that hillslopes in colder locations, both northward toward the LGM ice margin ( $\sim 41^{\circ}\text{N}$ ) and at higher elevations, have gentler gradients and are up to two times longer ( $\sim 1,000$  m) than those to the south and at lower elevations. Del Vecchio (2021) interpreted these findings as possible evidence of greater magnitudes and durations of frost cracking and thaw-induced sediment transport. These results mirror Pleistocene–Holocene palynological trends in the Appalachian region (Blois et al. 2011). With hillslope length as a proxy for the downslope extent of colluvium beyond sandstone-bearing ridge crests, Del Vecchio (2021) was able to test the ideas of earlier geologists who mapped colluvium and observed that its ridge to footslope transport distance increased northward (Denny 1951, 1956; Hack & Goodlett 1960; Ciolkosz et al. 1986a,b; Braun et al. 1994).

### Linking Relict Features with Modern Studies of Solifluction

We can further link studies of modern solifluction with relict features in the MAR. How long might it have taken to move sediment across Appalachian slopes via solifluction? If modern rates of solifluction movement are usually no more than 5.0 cm/year, and solifluction has moved sediment up to 1 km from source rocks during periglacial conditions, about 20 ky of transport is required. This is a somewhat surprisingly short time, given that periglacial conditions have occurred repeatedly during the Quaternary Period.

Perhaps most solifluction is concentrated during times of maximum permafrost degradation (Kirkby 1995), only a few thousand years after significantly cold periods. It is possible that as MAR slopes gradually became regolith mantled in response to Pleistocene cold-climate conditions, each cold episode resulted in continued reworking of older regolith already transported downslope. At upslope locations, cold-climate processes produced new regolith at the regolith–bedrock interface. Fresher regolith would then move downslope with and over older, reworked mobile regolith. As sediment moved downslope, hillslopes became longer and gentler (Del Vecchio 2021), enabling them to trap a substantial thickness of sediment transported from upslope.

Whereas the Hickory Run (Denn et al. 2017) and Garner Run (Del Vecchio et al. 2018) cosmogenic results revealed that boulder deposits on slopes are long-lived phenomena that accrue sediment and move downslope during multiple glacial cycles, the Palmerton lobe,  $\sim 20$  m from its source rock, indicates that fresh rock was produced by frost cracking moved downslope during the LGM (Merritts et al. 2020; D. Merritts, J. Marshall, R. Walter, M. Demitroff, N. Hertzler, et al., unpublished article). At that site, if sediment accrued by solifluction during a short period of late LGM permafrost thaw, perhaps 2,000 years, average flow rates would have been  $\sim 1$  cm/year, similar to modern rates.

What can be gleaned from comparisons of the size of relict solifluction features in the MAR with modern studies of solifluction? Glade et al. (2021) determined that lobe thickness for Norwegian solifluction lobes is correlated inversely with MAAT and positively with annual temperature



amplitude, with thicker lobes at lower temperatures and larger temperature amplitudes. Lobes in the MAR are up to ~9 m in thickness (see **Figures 2** and **15**), suggesting cold conditions and large temperature amplitudes. Their size is consistent with two-sided freezing and plug-like deformation. It also is possible that relict solifluction lobes and terraces in the MAR thicken with time because of boulder-rich fronts that stall flows and raise the permafrost table. Long-term reworking and remobilization of sediment by slope wash and frost creep during and after episodes of permafrost degradation as lobes become inactive are also likely to thicken periglacial deposits. The sizes of clasts within the solifluction lobe near Palmerton, Pennsylvania, shown in **Figure 15** (up to several meters), and thickness of individual layers (up to several meters) suggest transport associated with deep active layer thaw and possibly plug-like flow. This solifluction lobe and deposits within it are typical of those throughout the MAR along sandstone and orthoquartzite slopes.

## LEGACIES OF TIME EMBEDDED IN PERIGLACIAL LANDSCAPES

The MAR landscape is similar to an architectural palimpsest (e.g., an ancient cathedral), with some materials used over and over again and traces of older features underlying those that are more recent. Envisioning the transformation and repeated reshaping of mid-latitude landscapes due to cyclic cold conditions, Kirkby (1995) modeled regional variations in gelification rates under Pleistocene paleotemperature scenarios. Kirkby's conception of gelification processes includes both gelification and plug-like deformation described above, but not frost creep. His numerical modeling showed an equatorward shift of the region of active gelification during cold glacial conditions, with a relatively short (~2 ky) period of intense gelification during early postglacial warming and permafrost thaw. As noted above, permafrost formation periods at mid-latitudes probably were bracketed by episodes of deep seasonal freezing and ended with thaw-related geomorphic processes that modified, buried, or even destroyed evidence of former permafrost (Kirkby 1995, French et al. 2009). Modeling gelification as a diffusive process, Kirkby (1995) showed that hillslope forms were gradually rounded as mass shifted from upper convex parts to lower portions during intense gelification phases. Foothills generally became concave as they aggraded, resulting in typical convexo-concave hillslopes similar to those observed in formerly periglacial landscapes (Ballantyne 2018), including the MAR.

A view of the MAR as largely periglacial in origin and formerly underlain by permafrost, despite its modern temperate climate and vegetation cover, can inform current approaches to landscape restoration. Walter & Merritts (2008), for example, determined that MAR stream restoration was largely disconnected from understanding the geologic and climate history that accounted for unusual accumulations of coarse colluvium in valley bottoms. These sediments had previously been misinterpreted as mostly fluvial gravels. High Pleistocene periglacial sediment fluxes filled many valleys in the MAR, particularly those of lower order streams, with coarse sediment for which the coarsest fraction has been relatively immobile during the Holocene (Merritts et al. 2013, 2014; Chilton & Spotila 2020; Bodek et al. 2021). Yet, many restoration projects are designed to carry coarse sediment in valley bottoms with the premise that it is fluvial in origin (Merritts et al. 2011, 2013, 2014).

Paleoecologist Paul Martin (1958) recognized the significance of a periglacial legacy on valley bottoms at Great Marsh, Pennsylvania, a vast wetland complex about 40 km south of the LGM ice margin (Bricker & Moss 1958). Noting the rarity of pristine tussock sedge wet meadows in the region, Martin thought Great Marsh might be a late Pleistocene refugium. In one of the earliest uses of radiocarbon dating, Martin (1958) reported conventional radiocarbon ages of  $13,540 \pm 270$  and  $13,630 \pm 230$  years BP for organic soil samples from depths of ~1–1.6 m at



Great Marsh (calibrated  $^{14}\text{C}$  ages  $16,367 \pm 395$  and  $16,492 \pm 338$  years BP, respectively; OxCal 4.4). He identified pollen from this depth as indicative of taiga-tundra vegetation and correlated it with the time of the LGM. Observing that adjacent slopes are marked by relict periglacial boulder fields, Martin inferred that a modern analog for the LGM Great Marsh is the subarctic lysotundra, with “scattered trees in valleys surrounded by bare solifluction slopes” (Martin 1958, p. 470). Younger strata contained pollen that indicated a Holocene shift to tussock sedge wet meadow vegetation. The rarity of such wetlands today, as Walter & Merritts (2008) later showed, is not because they are late Pleistocene refugia. Rather, most Holocene valley bottom wetlands have been concealed by sediment trapped upstream of tens of thousands of historic (late seventeenth to early twentieth century) milldams in the MAR. One of the few locations with no milldams in the region, Great Marsh is a relict Holocene wetland landscape, watered by springs flowing from adjacent slopes mantled with frost-shattered bedrock and Pleistocene colluvium. Such is the legacy of formerly periglacial landscapes after permafrost thaw.

### SUMMARY POINTS

1. Most estimates of long-term erosion rates in the mid-Atlantic region (MAR) range from 10 to  $40\text{ m Myr}^{-1}$ , low enough that topographic and sedimentary legacies of frost cracking and other periglacial processes persist up to hundreds of thousands of years. Relict periglacial features include brecciated rock, thermal contraction crack polygon networks, frost wedges, and solifluction lobes and terraces.
2. Modern studies of thermal contraction cracking, frost cracking, and solifluction provide valuable analogs of periglacial processes, enhancing interpretations of relict features and paleoenvironmental conditions in the MAR. These show, for example, that highly brecciated rock to depths of nearly 10 m and widespread thermal contraction crack polygons are consistent with former permafrost and intense frost action.
3. Solifluction lobes on sandstone hillslopes in the MAR are large (up to  $\sim 9\text{ m}$  in height) and display fingering patterns that resemble fluid instabilities. Their size, and that of the boulders and bed thicknesses within them, is consistent with plug-like deformation, indicative of former permafrost. Spatial distribution of these relict features is co-located with other evidence of past LGM permafrost in the MAR.
4. Periglacial processes can account for most long-term erosion during the Quaternary Period. Given that  $\sim 10\text{--}20\text{ m}$  of colluvium (i.e., mobile regolith) has accumulated at footslopes throughout the region of permafrost extent in the MAR, upper slopes must have been lowered  $\sim 5\text{--}15\text{ m}$ , depending on rock to colluvium changes in bulk density.

### FUTURE ISSUES

1. Periglacial scientists have observed that published evidence on past periglacial environments in North America is slighter (and more recent) than that of similar work in Europe (Ballantyne 2018). In the past decade, significant advances that utilize high-resolution orthoimagery and lidar topographic data, cosmogenic nuclide analysis, and campaign-scale data gleaned from a multi-probe approach at the Susquehanna Shale Hills Observatory in central Pennsylvania have changed this status. Nevertheless, as the amount of evidence



accrues, an in-depth synoptic analysis of regional data is needed, particularly to better define the area of former permafrost extent.

2. Much could be gleaned about past climate conditions from careful analysis of the distribution and quantification of the dimensions of frost wedges, thermal contraction polygons, brecciated rock, and solifluction lobes in the MAR. Regional databases similar to those done in Europe (Bertran et al. 2014, Andrieux et al. 2016), with local attributes such as substrate, altitude, aspect, gradient, and data from cores, would enhance understanding of periglacial features, processes, and conditions.
3. Statistical analysis of morphometric data from remote sensing data, as with Mars research on thermal contraction polygons and solifluction lobes (Levy et al. 2009, Gallagher et al. 2011), could yield paleoclimate and other information for relict periglacial features in the MAR.
4. Modeling geomorphic processes in combination with paleoclimate simulations has great potential for further research on periglacial processes, landscape evolution, and climate conditions, as demonstrated in several recent studies (West et al. 2019, Del Vecchio 2021, Glade et al. 2021, Marshall et al. 2021).
5. The region's rich database of mapping from the US Geological Survey, state geological surveys, and US Department of Agriculture soil surveys, many of which contain details on surficial deposits, is likely to contain much information relevant to how landscapes have responded to warming and permafrost thaw over timescales of  $10^3$ – $10^4$  years.

## DISCLOSURE STATEMENT

The software used to make the terrain imagery in the Mapbox visualizations is part of Topomatrix LLC, owned by M.A.R.

## ACKNOWLEDGMENTS

For 10 years, an anonymous donor at Franklin and Marshall College has supported periglacial research in honor of John Moss and Dale Ritter, both former geomorphology professors at the college. Through this funding, we have been able to collaborate with numerous students and authors cited in this review. Another anonymous donor contributed support for costs of laboratory analyses, student research, and online visualizations built on Mapbox. We are grateful for this support. Many colleagues were generous with their time, insights, and feedback during compilation and analysis of literature. Particular gratitude goes to Robert Walter, Mark Demitroff, Duane Braun, Wayne Newell, Jill Marshall, Thomas Gardner, and George Gao, who provided significant assistance in locating and interpreting published reports and mapping, as well as in checking facts and reviewing parts of the text. Additional feedback from Noel Potter, Frank Pazzaglia, Joanmarie Del Vecchio, Steve Kite, Steve Grote, Scott Eaton, Stephen Wolfe, Sue Brantley, Roman DiBiase, Patrick Drohan, and Julian Murton was helpful and is much appreciated. Much gratitude goes to Joseph Levy, Mark Demitroff, Kevin Tammenga, and Patrick Drohan, who were helpful in obtaining photos to illustrate periglacial figures. The findings of many students and research associates at Franklin and Marshall College who have collaborated on this work have been essential to understanding the MAR's periglacial history. Special thanks go to Aaron Blair, Kayla Schulte, Samuel Alter, Ben Weiserbs, Evan Gross, John Ruck, Nic Hertzler, and Sam Feibel. Finally, we thank



all those whose work has led to our understanding of the marvelous, rich history of periglacial processes and features in the MAR.

## LITERATURE CITED

- Alter SR. 2015. *Periglacial Pennsylvania: evidence for periglacial processes and hillslope diffusion from the Last Glacial Maximum on Blue Mountain*. Honors Thesis, Franklin & Marshall Coll., Lancaster, PA. <https://digital.fandm.edu/object/scholars-square63291>
- Andersen JL, Egholm DL, Knudsen MF, Jansen JD, Nielsen SB. 2015. The periglacial engine of mountain erosion—part 1: rates of frost cracking and frost creep. *Earth Surf. Dyn.* 3(4):447–62
- Anderson RS. 1998. Near-surface thermal profiles in alpine bedrock: implications for the frost weathering of rock. *Arct. Alp. Res.* 30(4):362–72
- Anderson RS. 2002. Modeling the tor-dotted crests, bedrock edges, and parabolic profiles of high alpine surfaces of the Wind River Range, Wyoming. *Geomorphology* 46(1–2):35–58
- Anderson RS, Anderson SP, Tucker GE. 2013. Rock damage and regolith transport by frost: an example of climate modulation of the geomorphology of the critical zone. *Earth Surf. Proc. Landf.* 38(3):299–316
- Andersson JG. 1906. Solifluction, a component of subaerial denudation. *J. Geol.* 14:91–112
- Andrieux E, Bertran P, Saito K. 2016. Spatial analysis of the French Pleistocene permafrost by a GIS database. *Permafro. Periglac. Proc.* 27(1):17–30
- Ballantyne CK. 2018. *Periglacial Geomorphology*. Hoboken, NJ: John Wiley & Sons
- Ballantyne CK, Harris C. 1994. *The Periglaciation of Great Britain*. Cambridge, UK: Cambridge Univ. Press
- Batchelor CL, Margold M, Krapp M, Murton DK, Dalton AS, et al. 2019. The configuration of Northern Hemisphere ice sheets through the Quaternary. *Nat. Commun.* 10:3713
- Becher AE, Root SI. 1981. *Groundwater and Geology of the Cumberland Valley, Cumberland County*. Harrisburg, PA: Pa. Geol. Surv.
- Beerten K, Meylemans E, Kasse C, Mestdagh T, Van Rooij D, Bastiaens J. 2021. Networks of unusually large fossil periglacial polygons, Campine area, northern Belgium. *Geomorphology* 377:107582
- Behling RE, Kite JS, Springer TC, Cenderelli DA, Stuckenrath R. 1993. Buried organic-rich sediments in the unglaciated Appalachian Highlands: a stratigraphic model for finding pre-Late Wisconsin paleoenvironmental data. *Geol. Soc. Am. Abstr. Programs* 25:60
- Benedict JB. 1976. Frost creep and gelification features: a review. *Quat. Res.* 6(1):55–76
- Bertran P, Andrieux E, Antoine P, Coutard S, Deschodt L, et al. 2014. Distribution and chronology of Pleistocene permafrost features in France: database and first results. *Boreas* 43(3):699–711
- Black RF. 1976. Features indicative of permafrost. *Annu. Rev. Earth Planet. Sci.* 4:75–94
- Blois JL, Williams JW, Grimm EC, Jackson ST, Graham RW. 2011. A methodological framework for assessing and reducing temporal uncertainty in aleovegetation mapping from late-Quaternary pollen records. *Quat. Sci. Rev.* 30(15–16):1926–39
- Bodek S, Pizzuto JE, McCarthy KE, Affinito RA. 2021. Achieving equilibrium as a semi-alluvial channel: anthropogenic, bedrock, and colluvial controls on the White Clay Creek, PA, USA. *J. Geophys. Res. Earth Surf.* 126:e2020JF005920
- Brantley SL, White T, West N, Williams JZ, Forsythe B, et al. 2018. Susquehanna Shale Hills Critical Zone Observatory: shale hills in the context of Shaver's Creek watershed. *Vadose Zone J.* 17(1). <https://doi.org/10.2136/vzj2018.04.0092>
- Braun DD. 1989. Glacial and periglacial erosion of the Appalachians. *Geomorphology* 2(1–3):233–56
- Braun DD. 1996. *Surficial geology of the Nesquehoning 7.7' quadrangle, Carbon and Schuylkill Counties, Pennsylvania*. Open-File Rep. 96-25. Harrisburg, PA: Penn. Topogr. Geol. Surv.
- Braun DD. 2004. The glaciation of Pennsylvania, USA. *Dev. Quat. Sci.* 2:237–42
- Braun DD. 2011. The glaciation of Pennsylvania, USA. *Dev. Quat. Sci.* 15:521–29
- Braun DD, Ciolkosz EJ, Inners JD, Epstein JB. 1994. *Late Wisconsin to pre-Illinoian (G?) glacial and periglacial events in eastern Pennsylvania. Guidebook for the 57<sup>th</sup> Field Conference Friends of the Pleistocene Northeastern Section, May 20–22, 1994, Hazleton, Pennsylvania*. USGS Open-File Rep. 94-434. Reston, VA: US Geol. Surv.



- Bricker OP, Moss JH. 1958. Origin of the Marsh, East Nantmeal Township, Chester County, Pennsylvania. *Proc. Pa. Acad. Sci.* 32:168–71
- Burn CR. 1990. Implications for palaeoenvironmental reconstruction of recent ice-wedge development at Mayo, Yukon Territory. *Permafro. Periglac. Proc.* 1(1):3–14
- Carter BJ, Ciolkosz EJ. 1986. Sorting and thickness of waste mantle material on a sandstone spur in central Pennsylvania. *Catena* 13(3):241–56
- Chilton KD, Spotila JA. 2020. Preservation of Valley and Ridge topography via delivery of resistant, ridge-sourced boulders to hillslopes and channels, Southern Appalachian Mountains, USA. *Geomorphology* 365:107263
- Christiansen HH, Matsuoka N, Watanabe T. 2016. Progress in understanding the dynamics, internal structure and palaeoenvironmental potential of ice wedges and sand wedges. *Permafro. Periglac. Proc.* 27(4):365–76
- Ciolkosz EJ, Carter BJ, Hoover MT, Cronce RC, Waltman WJ, Dobos RR. 1990. Genesis of soils and landscapes in the Ridge and Valley province of central Pennsylvania. *Geomorphology* 3(3–4):245–61
- Ciolkosz EJ, Cronce RC, Cunningham RL, Petersen GW. 1986a. *Geology and soils of Nittany Valley*. Agronomy Ser. 88, Penn. State Univ., University Park. <https://ecosystems.psu.edu/research/labs/soilslife/pa-soils/pa-soils-information/publications/as88.pdf>
- Ciolkosz EJ, Cronce RC, Sevon WD. 1986b. *Periglacial features in Pennsylvania*. Agronomy Ser. 92. Penn. State Univ., University Park. <https://ecosystems.psu.edu/research/labs/soilslife/pa-soils/pa-soils-information/publications/as92.pdf>
- Clark GM. 1968. Sorted patterned ground: new Appalachian localities south of the glacial border. *Science* 161(3839):355–56
- Clark GM, Ciolkosz EJ. 1988. Periglacial geomorphology of the Appalachian Highlands and Interior Highlands south of the glacial border—a review. *Geomorphology* 1(3):191–220
- Clark PU, Dyke AS, Shakun JD, Carlson AE, Clark J, et al. 2009. The Last Glacial Maximum. *Science* 325(5941):710–14
- Conant LC, Black RF, Hosterman JW. 1976. Sediment-filled pots in upland gravels of Maryland and Virginia. *J. Res. U.S. Geol. Surv.* 4(3):353–58
- Costa JE, Cleaves ET. 1984. The Piedmont landscape of Maryland: a new look at an old problem. *Earth Surf. Proc. Landf.* 9(1):59–74
- Cronce RC. 1988. *The genesis of soils overlying dolomite in the Nittany Valley of central Pennsylvania*. PhD Diss. Penn. State Univ., State College
- Delcourt PA, Delcourt HR. 1981. Vegetation maps for eastern North America: 40,000 yr BP to the present. In *Geobotany II*, ed. RC Romans, pp. 123–65. New York: Plenum
- Del Vecchio J. 2021. *Appalachian pasts, Arctic futures: permafrost landscape response to warming*. PhD Diss. Penn. State Univ., State College
- Del Vecchio J, DiBiase RA, Corbett LB, Bierman PR, Caffee MW, Ivory SJ. 2021. Increased erosion rates following the onset of Pleistocene periglaciation at Bear Meadows, Pennsylvania, USA. *Geophys. Res. Lett.* 2021:e2021GL096739
- Del Vecchio J, DiBiase RA, Denn AR, Bierman PR, Caffee MW, Zimmerman SR. 2018. Record of coupled hillslope and channel response to Pleistocene erosion and deposition in a sandstone headwater valley, central Pennsylvania. *Geol. Soc. Am. Bull.* 130(11–12):1903–17
- Demitroff M. 2016. Pleistocene ventifacts and ice-marginal conditions, New Jersey, USA. *Permafro. Periglac. Proc.* 27:123–37
- Demitroff M, Doolittle JA, Nelson FE. 2008. Use of ground-penetrating radar to characterize cryogenic macrostructures in southern New Jersey, USA. In *Proceedings: Ninth International Conference on Permafrost*, Vol. 1, ed. DL Kane, KM Hinkel, pp. 355–60. Fairbanks, AK: Univ. Alaska Fairbanks
- Demitroff M, Wolfe SA, Woronko B, Chemieloska D, Cicili M. 2019. Late Pleistocene ice-marginal dune fields on the Atlantic Coastal Plain, New Jersey Pine Barrens, USA. *Geol. Soc. Am. Abstr. Programs* 51(5):188–4
- Denn AR, Bierman PR, Zimmerman SR, Caffee MW, Corbett LB, Kirby E. 2017. Cosmogenic nuclides indicate that boulder fields are dynamic, ancient, multigenerational features. *GSA Today* 28:4–10
- Denny CS. 1951. Pleistocene frost action near the border of the Wisconsin drift in Pennsylvania. *Ohio J. Sci.* 51(3):116–25



- Denny CS. 1956. *Surficial Geology and Geomorphology of Potter County, Pennsylvania*. Washington, DC: US Gov. Print. Off.
- Draebing D, Krautblatter M. 2019. The efficacy of frost weathering processes in alpine rockwalls. *Geophys. Res. Lett.* 46(12):6516–24
- Drohan PJ, Raab T, Hirsch F. 2020. Distribution of silty mantles in soils of the Northcentral Appalachians, USA. *Catena* 194:104701
- Duxbury J, Bierman PR, Portenga EW, Pavich MJ, Southworth S, Freeman SP. 2015. Erosion rates in and around Shenandoah National Park, Virginia, determined using analysis of cosmogenic  $^{10}\text{Be}$ . *Am. J. Sci.* 315(1):46–76
- Dyke AS, Moore A, Robertson L. 2003. *Deglaciation of North America*. Open File 1574. Ottawa, Can.: Geol. Surv. Can.
- Eaton LS, Morgan BA, Blair JL. 2001. *Surficial geologic map of the Fletcher, Madison, Stanardsville, and Swift Run Gap, 7.5-minute Quadrangles, Madison, Greene, Albemarle, Rockingham, and Page Counties, Virginia*. USGS Open-File Rep. 2001-92. Reston, VA: US Geol. Surv.
- Eaton LS, Morgan BA, Kochel RC, Howard AD. 2003a. Quaternary deposits and landscape evolution of the central Blue Ridge of Virginia. *Geomorphology* 56(1–2):139–54
- Eaton LS, Morgan BA, Kochel RC, Howard AD. 2003b. Role of debris flows in long-term landscape denudation in the central Appalachians of Virginia. *Geology* 31(4):339–42
- Egholm DL, Andersen JL, Knudsen MF, Jansen JD, Nielsen SB. 2015. The periglacial engine of mountain erosion—part 2: modelling large-scale landscape evolution. *Earth Surf. Dyn.* 3(4):463–82
- French H. 2003. The development of periglacial geomorphology: 1- up to 1965. *Permafri. Periglac. Proc.* 14(1):29–60
- French H. 2011. Frozen sediments and previously frozen sediments. *Geol. Soc. Lond. Spec. Publ.* 354:154–66
- French HM. 1979. Periglacial geomorphology. *Prog. Phys. Geogr.* 3(2):264–73
- French HM. 2000. Does Lozinski's periglacial realm exist today? A discussion relevant to modern usage of the term 'periglacial.' *Permafri. Periglac. Proc.* 11(1):35–42
- French HM. 2007. *The Periglacial Environment*. Chichester, UK: John Wiley & Sons. 3rd ed.
- French HM. 2008. Recent contributions to the study of past permafrost. *Permafri. Periglac. Proc.* 19:179–94
- French HM. 2016. Do periglacial landscapes exist? A discussion of the upland landscapes of northern interior Yukon, Canada. *Permafri. Periglac. Proc.* 27(2):219–28
- French HM. 2017a. The northern interior Yukon: an example of periglaciation. In *Landscapes and Landforms of Western Canada*, ed. O Slaymaker, pp. 257–66. Cham, Switz.: Springer
- French HM. 2017b. *The Periglacial Environment*. Hoboken, NJ: John Wiley & Sons. 4th ed.
- French HM, Demitroff M. 2001. Cold-climate origin of the enclosed depressions and wetlands ('spungs') of the Pine Barrens, southern New Jersey, USA. *Permafri. Periglac. Process.* 12:337–50
- French HM, Demitroff M. 2012. Late-Pleistocene paleohydrology, eolian activity and frozen ground, New Jersey Pine Barrens, eastern USA. *Neth. J. Geosci.* 91(1–2):25–35
- French HM, Demitroff M, Forman SL. 2003. Evidence for Late-Pleistocene permafrost in the New Jersey Pine Barrens (latitude 39°N), eastern USA. *Permafri. Periglac. Proc.* 14:259–74
- French HM, Demitroff M, Forman SL. 2005. Evidence for Late-Pleistocene thermokarst in the New Jersey Pine Barrens (latitude 39°N), eastern USA. *Permafri. Periglac. Proc.* 16:173–86
- French HM, Demitroff M, Forman SL, Newell WR. 2007. A chronology of Late-Pleistocene permafrost events in southern New Jersey, Eastern USA. *Permafri. Periglac. Proc.* 18:49–59
- French HM, Demitroff M, Newell WL. 2009. Past permafrost on the Mid-Atlantic Coastal Plain, eastern United States. *Permafri. Periglac. Proc.* 20:285–94
- French HM, Demitroff M, Streletsksiy D, Forman SL, Gozdzik J, et al. 2009b. [Evidence for Late-Pleistocene permafrost in the Pine Barrens, southern New Jersey]. *Earth's Cryosphere* 3:17–28 (In Russian)
- French HM, Millar SW. 2014. Permafrost at the time of the Last Glacial Maximum (LGM) in North America. *Boreas* 43(3):667–77
- French HM, Thorn CE. 2006. The changing nature of periglacial geomorphology. *Géomorphol. Relief Proc. Environ.* 12(3). <https://doi.org/10.4000/geomorphologie.119>



- Gallagher C, Balme MR, Conway SJ, Grindrod PM. 2011. Sorted clastic stripes, lobes and associated gullies in high-latitude craters on Mars: landforms indicative of very recent, polycyclic ground-ice thaw and liquid flows. *Icarus* 211(1):458–71
- Gao C. 2014. Relict thermal-contraction-crack polygons and past permafrost south of the Late Wisconsinan glacial limit in the mid-Atlantic Coastal Plain, USA. *Permafro. Periglac. Proc.* 25(2):144–49
- Gardner TW, Ritter JB, Shuman CA, Bell JC, Sasowsky KC, Pinter N. 1991. A periglacial stratified slope deposit in the valley and ridge province of central Pennsylvania, USA: sedimentology, stratigraphy, and geomorphic evolution. *Permafro. Periglac. Proc.* 2(2):141–62
- Geikie J. 1894. *The Great Ice Age*. London: Stanford. 3rd ed.
- Glade RC, Fratkin MM, Pouragha M, Seiphoori A, Rowland JC. 2021. Arctic soil patterns analogous to fluid instabilities. *PNAS* 118(21):e2101255118
- Goodfellow BW. 2012. A granulometry and secondary mineral fingerprint of chemical weathering in periglacial landscapes and its application to blockfield origins. *Quat. Sci. Rev.* 57:121–35
- Goodfellow BW, Boelhouwers J. 2013. Hillslope processes in cold environments: an illustration of high-latitude mountain and hillslope processes and forms. *Treatise Geomorphol.* 7:320–36
- Gooseff MN, Balser A, Bowden WB, Jones JB. 2009. Effects of hillslope thermokarst in northern Alaska. *Eos Trans. AGU* 90(4):29–30
- Gross ES. 2017. *Late Pleistocene climatic conditions inferred from sediment infill in a thermal-contraction wedge in shale bedrock near Carlisle, Pennsylvania*. Honors Thesis, Franklin & Marshall Coll., Lancaster, PA. <https://digital.fandm.edu/object/scholars-square2505>
- Grote T. 2017. Surficial processes and stratigraphy of alluvial fans along the Blue-Ridge-Great Valley border, south-central Pennsylvania. *Southeast. Geol.* 52(3):157–77
- Grote T, Kite JS. 2010. Geomorphology and pedology of a mixed alluvial-colluvial fill deposit in central West Virginia: new insight into Appalachian landscape evolution. *Southeast. Geol.* 47:27–39
- Gruber S. 2012. Derivation and analysis of a high-resolution estimate of global permafrost zonation. *Cryosphere* 6(1):221–33
- Gu X, Mavko G, Ma L, Oakley D, Accardo N, et al. 2020. Seismic refraction documents clay reactions and possible CO<sub>2</sub> production under a ridge and valley landscape. *PNAS* 117:18991–97
- Guo L, Chen J, Lin H. 2014. Subsurface lateral flow network on a hillslope revealed by time-lapse ground penetrating radar. *Water Resourc. Res.* 50:9127–47
- Hack JT, Goodlett JC. 1960. *Geomorphology and Forest Ecology of a Mountain Region in the Central Appalachians*. Washington, DC: US Gov. Print. Off.
- Hales TC, Roering JJ. 2007. Climatic controls on frost cracking and implications for the evolution of bedrock landscapes. *J. Geophys. Res.* 112(F2):F02033
- Hales TC, Roering JJ. 2009. A frost “buzzsaw” mechanism for erosion of the eastern Southern Alps, New Zealand. *Geomorphology* 107(3–4):241–53
- Hall K, Thorn CE, Matsuo N, Prick A. 2002. Weathering in cold regions: some thoughts and perspectives. *Prog. Phys. Geogr.* 26(4):577–603
- Hallet B, Walder JS, Stubbs CW. 1991. Weathering by segregation ice growth in microcracks at sustained subzero temperatures: verification from an experimental study using acoustic emissions. *Permafro. Periglac. Proc.* 2(4):283–300
- Hancock G, Kirwan M. 2007. Summit erosion rates deduced from <sup>10</sup>Be: implications for relief production in the central Appalachians. *Geology* 35(1):89–92
- Harris C. 2013. Slope deposits and forms. In *Encyclopedia of Quaternary Science*, Vol. 3, ed. S Elias, pp. 481–89. Amsterdam: Elsevier. 2nd ed.
- Harris C, Davies MC, Coutard JP. 1997. Rates and processes of periglacial solifluction: an experimental approach. *Earth Surf. Proc. Landf.* 22(9):849–68
- Harris C, Davies MC, Rea BR. 2003. Gelifluction: viscous flow or plastic creep? *Earth Surf. Proc. Landf.* 28(12):1289–301
- Harris C, Kern-Luetschg M, Christiansen HH, Smith F. 2011. The role of interannual climate variability in controlling solifluction processes, Endalen, Svalbard. *Permafro. Periglac. Process.* 22:239–55



- Harris C, Kern-Luetschg M, Murton J, Font M, Davies M, Smith F. 2008. Solifluction processes on permafrost and non-permafrost slopes: results of a large-scale laboratory simulation. *Permafro. Periglac. Proc.* 19(4):359–78
- Harris C, Rea B, Davies M. 2001. Scaled physical modelling of mass movement processes on thawing slopes. *Permafro. Periglac. Proc.* 12(1):125–35
- Hauber E, Reiss D, Ulrich M, Preusker F, Trauthan F, et al. 2011. Periglacial landscapes on Svalbard: terrestrial analogs for cold-climate landforms on Mars. *Geol. Soc. Am. Spec. Pap.* 483:177–201
- Head MJ. 2019. Formal subdivision of the Quaternary System/Period: present status and future directions. *Quat. Int.* 500:32–51
- Heginbottom JA, Brown J, Humlum O, Svensson H. 2012. *Permafrost and periglacial environments*. USGS Prof. Pap. 1386-A. Reston, VA: US Geol. Surv.
- Hertzler N. 2020. *Characteristics and origin of colluvial periglacial lobate landforms in the Pennsylvanian Appalachian Mountains*. Honors Thesis, Franklin & Marshall Coll., Lancaster, PA. <https://digital.fandm.edu/object/scholars-square52738>
- Hjort J. 2014. Which environmental factors determine recent cryoturbation and solifluction activity in a subarctic landscape? A comparison between active and inactive features. *Permafro. Periglac. Proc.* 25(2):136–43
- Holdgate MW, Allen SE, Chambers MJG. 1967. A preliminary investigation of the soils of Signy Island, South Orkney Islands. *Br. Antarct. Surv. Bull.* 12:53–71
- Jin L, Ravella R, Ketchum B, Bierman PR, Heaney P, et al. 2010. Mineral weathering and elemental transport during hillslope evolution at the Susquehanna/Shale Hills Critical Zone Observatory. *Geochim. Cosmochim. Acta* 74:3669–91
- Kinnard C, Lewkowicz AG. 2005. Movement, moisture and thermal conditions at a turf-banked solifluction lobe, Kluna Range, Yukon Territory, Canada. *Permafro. Periglac. Proc.* 16(3):261–75
- Kirkby MJ. 1995. A model for variations in gelification rates with temperature and topography: implications for global change. *Geogr. Ann. Ser. A Phys. Geogr.* 77(4):269–78
- Kite JS. 1987. Colluvial diamictons in the Valley and Ridge province, West Virginia and Virginia. *U.S. Geol. Surv. Circ.* 1008:21–23
- Kneller M, Peteet D. 1999. Late-glacial to early Holocene climate changes from a central Appalachian pollen and macrofossil record. *Quat. Res.* 51(2):133–47
- Kochel RC, Johnson RA. 1984. Geomorphology and sedimentology of humid-temperate alluvial fans, central Virginia. In *Sedimentology of Gravels and Conglomerates*, ed. EH Koster, RJ Steel, pp. 109–22. Calgary, Can.: Can. Soc. Petrol. Geol.
- Kuntz BW, Rubin S, Berkowitz B, Singha K. 2011. Quantifying solute transport at the Shale Hills Critical Zone Observatory. *Vadose Zone J.* 10(3):843–57
- Lachenbruch AH. 1962. *Mechanics of Thermal Contraction Cracks and Ice-Wedge Polygons in Permafrost*. New York: Geol. Soc. Am.
- Lachenbruch AH. 1966. Contraction theory of ice-wedge polygons: a qualitative discussion. In *International Permafrost Conference Publication 1287*, pp. 63–71. Lafayette, IN: Natl. Res. Counc.
- Lebedeva MI, Fletcher RC, Brantley SL. 2010. A mathematical model for steady-state regolith production at constant erosion rate. *Earth Surf. Proc. Landf.* 35(5):508–24
- Levy J, Head J, Marchant D. 2009. Thermal contraction crack polygons on Mars: classification, distribution, and climate implications from HiRISE observations. *J. Geophys. Res.* 114(E1):E01007
- Levy JS, Fountain AG, Goosseff MN, Welch KA, Lyons WB. 2011. Water tracks and permafrost in Taylor Valley, Antarctica: extensive and shallow groundwater connectivity in a cold desert ecosystem. *GSA Bull.* 123(11–12):2295–311
- Levy JS, Fountain AG, O'Connor JE, Welch KA, Lyons WB. 2013. Garwood Valley, Antarctica: a new record of Last Glacial Maximum to Holocene glacio-fluvial processes in the McMurdo Dry Valleys. *Geol. Soc. Am. Bull.* 125(9–10):1484–502
- Levy JS, Marchant DR, Head JW. 2006. Distribution and origin of patterned ground on Mullins Valley debris-covered glacier, Antarctica: the roles of ice flow and sublimation. *Antarct. Sci.* 18(3):385–97
- Lindeburg KS, Drohan PJ. 2019. Geochemical and mineralogical characteristics of loess along northern Appalachian, USA major river systems appear driven by differences in meltwater source lithology. *Catena* 172:461–68



- Lindgren A, Hugelius G, Kuhry P, Christensen TR, Vandenberghe J. 2016. GIS-based maps and area estimates of northern hemisphere permafrost extent during the Last Glacial Maximum. *Permafrost Periglac Proc.* 27(1):6–16
- Litwin RJ, Smoot JP, Pavich MJ, Markewich HW, Brook G, Durka NJ. 2013. 100,000-year-long terrestrial record of millennial-scale linkage between eastern North American mid-latitude paleovegetation shifts and Greenland ice-core oxygen isotope trends. *Quat. Res.* 80(2):291–315
- Lorenz DJ, Nieto-Lugilde D, Blois JL, Fitzpatrick MC, Williams JW. 2016. Downscaled and debiased climate simulations for North America from 21,000 years ago to 2100AD. *Sci. Data* 3(1):160048
- Ma L, Chabaux F, Pelt E, Blaes E, Jin L, Brantley S. 2010. Regolith production rates calculated with uranium-series isotopes at Susquehanna/Shale Hills Critical Zone Observatory. *Earth Planet. Sci. Lett.* 297(1–2):211–25
- Ma L, Chabaux F, West N, Kirby E, Jin L, Brantley S. 2013. Regolith production and transport in the Susquehanna Shale Hills Critical Zone Observatory, part 1: insights from U-series isotopes. *J. Geophys. Res. Earth Surf.* 118(2):722–40
- Ma L, Oakley D, Nyblade A, Moon S, Accardo N, et al. 2021. Seismic imaging of a shale landscape under compression shows limited influence of topography-induced fracturing. *Geophys. Res. Lett.* 48(17):e2021GL093372
- Mackay JR. 1974. Ice-wedge cracks, Garry Island, Northwest Territories. *Can. J. Earth Sci.* 11(10):1366–83
- Mackay JR. 1981. Active layer slope movement in a continuous permafrost environment, Garry Island, Northwest Territories, Canada. *Can. J. Earth Sci.* 18(11):1666–80
- Mackay JR. 1993. Air temperature, snow cover, creep of frozen ground, and the time of ice-wedge cracking, western Arctic coast. *Can. J. Earth Sci.* 30(8):1720–29
- Mackay JR. 1999. Cold-climate shattering (1974 to 1993) of 200 glacial erratics on the exposed bottom of a recently drained arctic lake, Western Arctic coast, Canada. *Permafrost Periglac Proc.* 10(2):125–36
- Mackay JR, Burn CR. 2002. The first 20 years (1978–1979 to 1998–1999) of ice-wedge growth at the Illisarvik experimental drained lake site, western Arctic coast, Canada. *Can. J. Earth Sci.* 39(1):95–111
- Marsh B. 1987. Pleistocene pingo scars in Pennsylvania. *Geology* 15(10):945–47
- Marsh B. 1998. Wind-transverse corrugations in Pleistocene periglacial landscapes of central Pennsylvania. *Quat. Res.* 49(2):149–56
- Marsh B. 1999. *Paleoperiglacial Landscapes of Central Pennsylvania: Sixty-Second Annual Reunion, Northeast Friends of the Pleistocene*. Lewisburg, Pa.: Bucknell Univ.
- Marshall JA, Roering JJ, Bartlein PJ, Gavin DG, Granger DE, et al. 2015. Frost for the trees: Did climate increase erosion in unglaciated landscapes during the late Pleistocene? *Sci. Adv.* 1(10):e1500715
- Marshall JA, Roering JJ, Gavin DG, Granger DE. 2017. Late Quaternary climatic controls on erosion rates and geomorphic processes in western Oregon, USA. *Geol. Soc. Am. Bull.* 129(5–6):715–31
- Marshall JA, Roering JJ, Rempel AW, Shafer SL, Bartlein PJ. 2021. Extensive frost weathering across unglaciated North America during the Last Glacial Maximum. *Geophys. Res. Lett.* 48(5):e2020GL090305
- Martin PS. 1958. Taiga-tundra and the full-glacial period in Chester County, Pennsylvania. *Am. J. Sci.* 256:470–502
- Matsuoka N. 2001. Solifluction rates, processes and landforms: a global review. *Earth-Sci. Rev.* 55(1–2):107–34
- Matsuoka N, Murton J. 2008. Frost weathering: recent advances and future directions. *Permafrost Periglac Proc.* 19(2):195–210
- Maxwell JA, Davis MB. 1972. Pollen evidence of Pleistocene and Holocene vegetation on the Allegheny Plateau, Maryland. *Quat. Res.* 2(4):506–30
- Merritts D, Schulte K, Blair A, Potter N, Walter R, et al. 2014. Lidar analysis of periglacial landforms and their paleoclimatic significance, unglaciated Pennsylvania. In *Guidebook for the Annual Field Conference of Pennsylvania Geologists*, Vol. 79, ed. R Anthony, DM Hoskins, N Potter, pp. 49–72. Harrisburg, PA: Field Conf. Pa. Geol.
- Merritts D, Walter R, Rahnis M, Cox S, Hartranft J, et al. 2013. The rise and fall of Mid-Atlantic streams: millpond sedimentation, milldam breaching, channel incision, and stream bank erosion. *Rev. Eng. Geol.* 21:183–203



- Merritts D, Walter R, Rahnis M, Hartranft J, Cox S, et al. 2011. Anthropocene streams and base-level controls from historic dams in the unglaciated mid-Atlantic region, USA. *Philos. Trans. R. Soc. A* 369:1938:976–1009
- Merritts DJ, Walter RC, Blair A, Demitroff M, Potter N Jr., et al. 2015. LIDAR, orthoimagery, and field analysis of periglacial landforms and their cold climate signature, unglaciated Pennsylvania and Maryland. *Geol. Soc. Am. Abstr. Programs* 47(7):831
- Merritts DJ, Walter RC, Ruck J, Hertzler N, Barter R, Jean J. 2020. Mapping the last permafrost maximum boundary south of the last glacial maximum ice margin, eastern US Appalachian region. *Geol. Soc. Am. Abstr. Programs* 52(6):250–2
- Middlekauff BD. 1991. Probable paleoperiglacial morphosequences in the northern Blue Ridge. *Phys. Geogr.* 12(1):19–36
- Miller SR, Sak PB, Kirby E, Bierman PR. 2013. Neogene rejuvenation of central Appalachian topography: evidence for differential rock uplift from stream profiles and erosion rates. *Earth Planet. Sci. Lett.* 369:1–12
- Mills HH. 1981. Boulder deposits and the retreat of mountain slopes, or, “gully gravure” revisited. *J. Geol.* 89(5):649–60
- Moss JH. 1976. Periglacial origin of extensive lobate colluvial deposits on the south flank of Blue Mountain near Shartlesville and Strausstown, Berks County, Pennsylvania. *Proc. Pa. Acad. Sci.* 50:42–44
- Murton JB. 1996. Near-surface brecciation of chalk, Isle of Thanet, South-East England: a comparison with ice-rich brecciated bedrocks in Canada and Spitsbergen. *Permafri. Periglac. Proc.* 7(2):153–64
- Murton JB. 2013. Ice wedges and ice-wedge casts. In *Encyclopedia of Quaternary Science*, Vol. 3, ed. SA Elias, CJ Mock, pp. 436–51. Amsterdam: Elsevier. 2nd ed.
- Murton JB. 2021a. Periglacial processes and deposits. In *Encyclopedia of Geology*, Vol. 2, ed. D Alderton, SA Elias SA, pp. 857–75. London: Academic Press. 2nd ed.
- Murton JB. 2021b. What and where are periglacial landscapes? *Permafri. Periglac. Proc.* 32(2):186–212
- Murton JB, Ballantyne CK. 2017. Periglacial and permafrost ground models for Great Britain. *Geol. Soc. Lond.* 28(1):501–97
- Murton JB, Coutard JP, Lautridou JP, Ozouf JC, Robinson DA, Williams RBG. 2001. Physical modelling of bedrock brecciation by ice segregation in permafrost. *Permafri. Periglac. Proc.* 12(3):255–66
- Murton JB, Peterson R, Ozouf JC. 2006. Bedrock fracture by ice segregation in cold regions. *Science* 314(5802):1127–29
- Murton JB, Worsley P, Gozdzik J. 2000. Sand veins and wedges in cold aeolian environments. *Quat. Sci. Rev.* 19(9):899–922
- Nelson KJP, Nelson FE, Walegur MT. 2007. Periglacial Appalachia: palaeoclimatic significance of blockfield elevation gradients, eastern USA. *Permafri. Periglac. Proc.* 18(1):61–73
- Newell WL. 2005. *Evidence of cold climate slope processes from the New Jersey Coastal Plain: debris flow stratigraphy at Haines Corner, Camden County, New Jersey*. USGS Open-File Rep. 2005-1296. Reston, VA: US Geol. Surv.
- Newell WL, DeJong BD. 2011. Cold-climate slope deposits and landscape modifications of the Mid-Atlantic Coastal Plain, eastern USA. *Geol. Soc. Lond. Spec. Publ.* 354(1):259–76
- Newell WL, Powars DS, Owens JP, Stanford SD, Stone BD. 2000. *Surficial geologic map of central and southern New Jersey*. USGS Misc. Investig. Ser. Map 1-2540-D. Reston, VA: US Geol. Surv.
- Newell WL, Wyckoff JS, Owens JP, Farnsworth J. 1989. *2nd Southeast Friends of the Pleistocene, annual field conference: Cenozoic geology and geomorphology of southern New Jersey Coastal Plain, November 11–13, 1988*. USGS Open-File Rep.89-159. Reston, VA: US Geol. Surv.
- Nikiforoff CC. 1955. *Hardpan Soils of the Coastal Plain of Southern Maryland*. Washington, DC: US Gov. Print. Off.
- Otvos EG. 2015. The last interglacial stage: definitions and marine highstand, North America and Eurasia. *Quat. Int.* 383:158–73
- Pazzaglia FJ, Braun DD, Pavich M, Bierman P, Potter N, et al. 2006. Rivers, glaciers, landscape evolution, and active tectonics of the central Appalachians, Pennsylvania and Maryland. In *Excursions in Geology and History: Field Trips in the Middle Atlantic States*, Vol. 8, ed. FJ Pazzaglia, pp. 169–97. Boulder, CO: Geol. Soc. Am.



- Pazzaglia FJ, Cleaves ET. 1998. *Surficial Geology of the Delta Quadrangle, Harford County, Maryland and York County, Pennsylvania*. Baltimore, MD: Md. Geol. Surv.
- Peltier LC. 1949. *Pleistocene Terraces of the Susquehanna River, Pennsylvania*. Harrisburg, PA: Bur. Topogr. & Geol. Surv.
- Peltier LC. 1950. The geographic cycle in periglacial regions as it is related to climatic geomorphology. *Ann. Assoc. Am. Geogr.* 40(3):214–36
- Peteet DM, Beh M, Orr C, Kurdyla D, Nichols J, Guilderson T. 2012. Delayed deglaciation or extreme Arctic conditions 21–16 cal. kyr at southeastern Laurentide Ice Sheet margin? *Geophys. Res. Lett.* 39(11):L11706
- Péwé R, Brown T. 1973. Distribution of permafrost in North America and its relationship to the environment: a review, 1963–1973. In *Permafrost: North American Contribution [to the] Second International Conference*, Vol. 2, pp. 71–100. Washington, DC: Natl. Acad. Sci.
- Péwé TL. 1983. The periglacial environment in North America during Wisconsin time. In *The Late Quaternary Environments of the United States*, Vol. 1, ed. HE Wright, SC Porter, pp. 157–89. Minneapolis: Univ. Minn. Press
- Plug LJ, Werner BT. 2001. Fracture networks in frozen ground. *J. Geophys. Res.* 106(B5):8599–613
- Plug LJ, Werner BT. 2008. Modelling of ice-wedge networks. *Permafri: Periglac. Proc.* 19(1):63–69
- Portenga EW, Bierman PR. 2011. Understanding Earth's eroding surface with  $^{10}\text{Be}$ . *GSA Today* 21:4–10
- Portenga EW, Bierman PR, Rizzo DM, Rood DH. 2013. Low rates of bedrock outcrop erosion in the central Appalachian Mountains inferred from in situ  $^{10}\text{Be}$ . *GSA Bull.* 125(1–2):201–15
- Portenga EW, Bierman PR, Trodick CD Jr., Greene SE, DeJong BD, et al. 2019. Erosion rates and sediment flux within the Potomac River basin quantified over millennial timescales using beryllium isotopes. *Geol. Soc. Am. Bull.* 131(7–8):1295–311
- Potter N Jr., Moss JH. 1968. Origin of the Blue Rocks block field and adjacent deposits, Berks County, Pennsylvania. *Geol. Soc. Am. Bull.* 79(2):255–62
- Rempel AW, Marshall JA, Roering JJ. 2016. Modeling relative frost weathering rates at geomorphic scales. *Earth Planet. Sci. Lett.* 453:87–95
- Ridefelt H, Åkerman J, Beylich AA, Boelhouwers J, Kolstrup E, Nyberg R. 2009. 56 years of solifluction measurements in the Abisko Mountains, northern Sweden—analysis of temporal and spatial variations of slow soil surface movement. *Geogr. Ann.* 91(3):215–32
- Riggins SG, Anderson RS, Anderson SP, Tye AM. 2011. Solving a conundrum of a steady-state hilltop with variable soil depths and production rates, Bodmin Moor, UK. *Geomorphology* 128(1–2):73–84
- Rowland JC, Jones CE, Altmann G, Bryan R, Crosby BT, et al. 2010. Arctic landscapes in transition: responses to thawing permafrost. *Eos Trans. AGU* 91(26):229–30
- Ruck J. 2020. *Properties and mechanisms of transport of colluvial sediment in relict lobate landforms on hillslopes south of the Last Glacial Maximum ice margin, Pennsylvania, and possible association with Late Pleistocene permafrost*. Honors Thesis, Franklin & Marshall Coll., Lancaster, PA. <https://digital.fandm.edu/object/scholars-square52739>
- Ruck J, Hertzler N, Merritts DJ, Walter RC, Marshall JA, et al. 2020. Field and cosmogenic nuclide studies of possible Last Glacial Maximum gelifluction benches in northeastern Pennsylvania. *Geol. Soc. Am. Abstr. Programs* 52(2):7–11
- Sevon WD. 1987. The Hickory Run boulder field, a periglacial relict, Carbon County, Pennsylvania. *North-eastern Section of the Geological Society of America Centennial Field Guide*, Vol. 5, ed. DC Roy, pp. 75–76, Boulder, CO: Geol. Soc. Am.
- Sevon WD, Braun DD. 2000. *Map 59: Glacial Deposits of Pennsylvania*. Harrisburg, PA: Bur. Topogr. & Geol. Surv.
- Shafer SL, Bartlein PJ, Izumi K. 2021. *PMIP3/CMIP5 LGM simulated temperature data on a North America 10-km grid, version 1.0*. USGS. Data Release, <https://doi.org/10.5066/P9KC0L47>
- Slim M, Perron JT, Martel SJ, Singha K. 2015. Topographic stress and rock fracture: a two-dimensional numerical model for arbitrary topography and preliminary comparison with borehole observations. *Earth Surf. Proc. Landf.* 40(4):512–29
- Smith HTU. 1953. The Hickory Run boulder field, Carbon County, Pennsylvania. *Am. J. Sci.* 251(9):625–42
- Smoot J. 2004. *Sedimentary fabrics of stratified slope deposits at a site near Hoover's Camp, Shenandoah National Park, Virginia*. USGS Open-File Rep. 1059-52. Reston, VA: US Geol. Surv.



- Snyder KE, Bryant RB. 1992. Late Pleistocene surficial stratigraphy and landscape development in the Salamanca Re-entrant, southwestern New York. *Geol. Soc. Am. Bull.* 104(2):242–51
- Sullivan PL, Hynek SA, Gu X, Singha K, White T, et al. 2016. Oxidative dissolution under the channel leads geomorphological evolution at the Shale Hills catchment. *Am. J. Sci.* 316(10):981–1026
- Taylor SB, Kite JS. 2006. Comparative geomorphic analysis of surficial deposits at three central Appalachian watersheds: implications for controls on sediment-transport efficiency. *Geomorphology* 78(1–2):22–43
- Thomson CW. 1878. *The Atlantic: A Preliminary Account of the General Results of the Exploring Voyage of HMS Challenger*. New York: Harper & Brothers
- Thorn CE. 1992. Periglacial geomorphology: what, where, when? In *Periglacial Geomorphology*, ed. JC Dixon, AD Abrahams, pp. 1–30. London: Routledge
- Vandenberghhe J, French HM, Gorbunov A, Marchenko S, Velichko AA, et al. 2014. The Last Permafrost Maximum (LPM) map of the Northern Hemisphere: permafrost extent and mean annual air temperatures, 25–17 ka BP. *Boreas* 43(3):652–66
- Verpaelst M, Fortier D, Kanevskiy M, Paquette M, Shur Y. 2017. Syngenetic dynamic of permafrost of a polar desert solifluction lobe, Ward Hunt Island, Nunavut. *Arct. Sci.* 3(2):301–19
- Vlahou I, Worster MG. 2015. Freeze fracturing of elastic porous media: a mathematical model. *Proc. R. Soc. A* 471(2175):20140741
- von Loziński W. 1909. Über die mechanische Verwitterung der Sandsteine im gemässigten klima. *Bull. Int. l'Acad. Sci. Cracov. Class Sci. Math. Nat.* 1:1–25 [English translation: Mrozek T. 1994. On the mechanical weathering of sandstones in temperate climates. In *Cold Climate Landforms*, ed. DJE Evans, pp. 119–34. Chichester, UK: John Wiley & Sons]
- von Loziński W. 1912. Die periglaziales fazies der mechanischen Verwitterung. In *Comptes Rendus, XI Congrès Internationale Géologie*, pp. 1039–53. Stockholm
- Walder J, Hallet B. 1985. A theoretical model of the fracture of rock during freezing. *Geol. Soc. Am. Bull.* 96(3):336–46
- Walder JS, Hallet B. 1986. The physical basis of frost weathering: toward a more fundamental and unified perspective. *Arct. Alp. Res.* 18(1):27–32
- Walter RC, Merritts DJ. 2008. Natural streams and the legacy of water-powered mills. *Science* 319(5861):299–304
- Walters JC. 1978. Polygonal patterned ground in central New Jersey. *Quat. Res.* 10(1):42–54
- Washburn AL. 1980. *Geocryology: A Survey of Periglacial Processes and Environments*. New York: Wiley
- Watts WA. 1979. Late Quaternary vegetation of central Appalachia and the New Jersey coastal plain. *Ecol. Monogr.* 49(4):427–69
- West N, Kirby E, Bierman P, Rood D. 2011. Preliminary estimates of regolith generation and mobility in the Susquehanna Shale Hills Critical Zone Observatory, Pennsylvania, using meteoric  $^{10}\text{Be}$ . *Appl. Geochem.* 26:S146–48
- West N, Kirby E, Bierman P, Clarke BA. 2014. Aspect-dependent variations in regolith creep revealed by meteoric  $^{10}\text{Be}$ . *Geology* 42(6):507–10
- West N, Kirby E, Bierman P, Slingerland R, Ma L, et al. 2013. Regolith production and transport at the Susquehanna Shale Hills Critical Zone Observatory, part 2: insights from meteoric  $^{10}\text{Be}$ . *J. Geophys. Res. Earth Surf.* 118(3):1877–96
- West N, Kirby E, Nyblade AA, Brantley SL. 2019. Climate preconditions the critical zone: elucidating the role of subsurface fractures in the evolution of asymmetric topography. *Earth Planet. Sci. Lett.* 513:197–205
- Whittecac GR, Wynn TC, Bartlett CS. 2007. Paleoenvironmental analysis of a middle Wisconsinan biota site, southwestern Virginia, USA. *Quat. Res.* 68(1):133–40
- Wilson P, Bentley MJ, Schnabel C, Clark R, Xu S. 2008. Stone run (block stream) formation in the Falkland Islands over several cold stages, deduced from cosmogenic isotope ( $^{10}\text{Be}$  and  $^{26}\text{Al}$ ) surface exposure dating. *J. Quat. Sci.* 23(5):461–73
- Wolfe SA, Morse PD, Neudorf CM, Kokelj SV, Lian OB, O'Neill HB. 2018. Contemporary sand wedge development in seasonally frozen ground and paleoenvironmental implications. *Geomorphology* 308:215–29

